The calcium binding protein S100β marks Hedgehog-responsive perivascular stem cells that contribute to intimal thickening following iatrogenic flow restriction

¶Mariana Di Luca[1], ¶Emma Fitzpatrick[1], ¶Denise Burtenshaw[1], ¶Weimin Liu[2], Jay-Christian Helt[2], Roya Hakimjavadi[1], Eoin Corcoran[1], Yusof Gusti[1], Daniel Sheridan[1], Susan Harman[1], Catriona Lally[3], Eileen M. Redmond[2], and Paul A. Cahill*[1]

[1] Dublin City University, Vascular Biology & Therapeutics Group, School of Biotechnology (Dublin, Ireland); [2] University of Rochester, Dept Surgery (Rochester, New York, United States) [3]Trinity College Dublin, Trinity Centre for Bioengineering, Trinity Biomedical Sciences Institute, (Dublin, Ireland).

¶ Contributed equally

*Address for correspondence

Paul A. Cahill., BSc., PhD
Professor, School of Biotechnology
Chair of Vascular Biology & Therapeutics, School of Biotechnology
Londsdale Bldg, Office X2-09, Faculty of Science and Health
Dublin City University, Glasnevin, Dublin 9. Ireland
E: paul.cahill@dcu.ie, Ph: 353-1-700-8466, Fax: 353-1-700-5412

Summary

The origin(s) of smooth muscle-like cells contributing to the development of subclinical arteriosclerosis remains controversial. Using Sca1-eGFP and S100β-eGFP transgenic mice together with genetic lineage tracing of S100β$^+$ vascular stem cells (vSCs), we identified a S100β$^+$/Sca1$^+$ population, originating from a perivascular non-smooth muscle cell (SMC) S100β$^+$ parent population in lesions developed following iatrogenic flow restriction. Neuroectoderm S100β$^+$ vSCs isolated from atheroprone murine vessels were Hedgehog (Hh) responsive, enriched for the trimethylation of lysine 27 at histone 3 (H3K27me3) repressive mark at the Myh11 locus, and underwent myogenic differentiation *in vitro.* Inhibition of Hh signalling reduced the number of S100β$^+$/Sca1$^+$ cells and attenuated lesion formation. Hh promoted myogenic differentiation of S100β$^+$ vSCs derived from human induced pluripotent stem cells (iPSC) *in vitro,* while S100β$^+$ cells were enriched in human lesions. We conclude that Hh-responsive S100β vSC-derived progeny contribute to adaptive lesions and support targeting Hh signalling to treat subclinical arteriosclerosis.

Keywords: Arteriosclerosis, intimal thickening, resident vascular stem cells, S100β calcium binding proteins, stem cell antigen-1, lineage tracing, hedgehog signalling, human induced pluripotent stem cells (HiPSCs).

Introduction

Atherosclerosis is a chronic progressive inflammatory disease that leads to myocardial infarction and stroke (Bennett et al., 2016). Pathologic observations in humans vessels confirm that early 'transitional' lesions enriched with smooth muscle (SMC)-like cells are routinely present in atherosclerotic-prone regions of arteries before pathologic intimal thickening, lipid retention, and the appearance of a developed plaque (Sakamoto et al., 2018). Endothelial cell (EC) dysfunction due to disturbed blood flow is classically associated with the development of atheroprone lesions (Halcox et al., 2009; Hromada et al., 2017; Zhang et al., 2013), while the embryological origin (e.g., neuroectoderm versus mesoderm) of SMCs may also influence disease localisation and progression (Sinha et al., 2014). These early lesions represent an important therapeutic target and are routinely modelled in mouse carotid arteries following flow restriction due to ligation (Korshunov and Berk, 2003). These ligation-induced lesions can further develop into advanced atherosclerotic plaques in *ApoE* knockout mice on Western diets (Liu et al., 2011; Nam et al., 2009).

Since 2011, several groups have used cell fate mapping with myosin heavy chain 11 (Myh11)-CreERT2 mice to indelibly mark vascular SMCs within the vessel wall and track their progeny to determine their contribution to intimal thickening using various injury models (Chappell et al., 2016; Herring et al., 2014; Nemenoff et al., 2011; Shankman et al., 2015). These studies provided compelling evidence for the involvement of a population of differentiated Myh11$^+$ medial SMC in progressing intimal thickening (Shi et al., 2019). A study using single cell RNA sequence analysis (scRNA-seq) suggested that a stem cell antigen-1 positive (Sca1$^+$) Myh11-Cre marked SMC subpopulation gives rise to neointimal cells during disease progression (Dobnikar et al., 2018).

Several vascular progenitors have been identified within the vessel wall in both humans and rodents (Zhang et al., 2018). In particular, the adventitia, which displays increased cell proliferation and inflammation following injury (Seidelmann et al., 2014), contains a heterogeneous population of progenitor/precursor cells with the majority of them expressing Sca1 (Fitzpatrick et al., 2017; Passman et al., 2008; Shikatani et al., 2016; Wan et al., 2012). Recent cell fate mapping and scRNA-seq studies implicate adventitial Sca1$^+$ cells in generating

de novo neointimal SMC-like cells that expand more efficiently than pre-existing SMCs (Tang et al., 2020). Those findings extend previous lineage tracing analysis of non-SMCs within the vessel wall using Cre-LoxP that provided evidence for a role of adventitial and medial progenitors in progressing intimal thickening (Baker and Péault, 2016; Kramann et al., 2016; Majesky et al., 2017; Schneider et al., 2018; Wan et al., 2012; Yuan et al., 2017). While some adventitial progenitors are derived from a parent Myh11$^+$ SMC population (Majesky et al., 2017), SRY-related HMG-box 10 positive (Sox10$^+$) adventitial/medial resident multipotent vSCs, and Nestin$^+$ progenitor cells have also been shown to contribute to neointimal thickening (Wan et al., 2012; Yuan et al., 2017). Despite these insights, the putative role of resident vascular stem cells that do not originate from medial Myh11$^+$ SMCs in promoting intimal thickening remains controversial. Moreover, the molecular signals that control the fate of resident vascular cells and their myogenic progeny during the progression of early transitional lesions are unknown.

S100β, a member of the S100 multigenic family expressing small (9 kDa and 14 kDa) Ca2+-binding proteins of the EF-hand type, is primarily localised to astrocytes and glial cells under normal physiological conditions and is positively associated with age and various neurodegenerative and neuroinflammatory diseases (Donato et al., 2009). S100β promotes intimal thickening through interaction with the receptor for advanced glycation end-products (RAGE) (Cao et al., 2017) and induces migration and infiltration of inflammatory cells associated with cerebral ischemic disease and muscular dystrophy (Sagheddu et al., 2018; Zhou et al., 2018). Importantly, S100β appears to play a crucial role in maintaining an intermediate state of Sca1$^+$ progenitor cells following injury-induced neointimal thickening through a RAGE and stromal cell-derived factor-1 α/CXCR4 signalling mechanism (Wu et al., 2019).

Genome-wide association studies have identified chromosome 14q32 as a locus for coronary artery disease (López-Mejías et al., 2017). The disease-associated variants fall in a hitherto uncharacterized gene called HHIPL1 (hedgehog interacting protein-like 1), which encodes a sequence homolog of an antagonist of hedgehog signalling that is secreted as a pro-atherogenic protein to regulate SMC proliferation and migration (Aravani et al., 2019). A role for sonic hedgehog (SHh) signalling in influencing pathologic vascular remodeling is supported in the literature. Canonical signalling begins when SHh binds to the Ptch1 receptor resulting in the removal of its' inhibitory effect on the smoothened (SMO) receptor subsequently allows Gli

family transcription factors to translocate to the nucleus and effect the expression of Hh target genes, including Gli1, Gli2, and Ptch1 (Briscoe and Thérond, 2013). Hh signalling is blocked with inhibitors like cyclopamine that bind to SMO preventing it from signalling downstream, or with small molecule Hh pathway inhibitors (HPIs) that act downstream of SMO (Hyman et al., 2009). In atherosclerotic mice, Hh has a permissive role through increased lipid uptake by macrophages (Beckers et al., 2007), while global Hhipl1 deletion reduces plaque burden in atherosclerotic mice (Aravani et al., 2019). Hh signalling, especially SHh and signal peptide CUB domain and EGF like domain containing 2 (Scube2), are overexpressed in injured arteries notably during lesion formation after flow restriction (Ali et al., 2013; Dutzmann et al., 2017; Morrow et al., 2009), autogenous vein grafts (Li et al., 2010), and hypoxic pulmonary arterial SMCs (Wang et al., 2010). Importantly, adventitial Sca1 cells that co-localise with SHh and Ptch1 (Passman et al., 2008) significantly contribute to intimal thickening *in vivo* (Dutzmann et al., 2017; Shikatani et al., 2016; Tsai et al., 2012) while local perivascular depletion of Ptch1 attenuates intimal thickening following iatrogenic flow-restriction *in vivo* (Redmond et al., 2013).

Given the putative role of Hh in controlling stem cell fate during development (Briscoe and Thérond, 2013) and atherogenesis (Aravani et al., 2019), we sought to determine whether Hh responsive S100β/Sca1 stem cells contribute to intimal thickening and the progression of adaptive lesions *in vivo* and, furthermore, whether Hh signalling directs murine S100β$^+$ resident vascular stem cells and human induced pluripotent stem cell (hiPSC)-derived S100β$^+$ neuroectoderm stem cells to undergo myogenic differentiation *in vitro*.

Results

Perivascular Sca1$^+$ and S100β$^+$ stem cells are present in normal adult murine vessels

The presence of perivascular Sca1$^+$ cells was first investigated in whole mounted murine aorta and carotid arteries from Sca1-eGFP mice (Ma et al., 2002). A discrete number of Sca1-eGFP cells were present on collagen fibres within the adventitial layer of the thoracic aorta and carotid artery, when compared to wild-type (WT) controls [Suppl Figure 1A, B]. The cells were located predominantly at the aortic arch and at bifurcations with intercostal vessels, and their presence diminished within the descending and abdominal aorta [Suppl Figure 1C]. In arteries from

S100β-eGFP mice (Hayashi et al., 2007), a discrete number of perivascular S100β$^+$ cells were present on collagen fibres within the adventitial layer of the aortic arch and thoracic aorta, and their presence similarly diminished along the descending and abdominal aorta [Suppl Figure 1D]. These data confirm that Sca1$^+$ and S100β$^+$ cells are present in perivascular regions of normal arterial vessels *in vivo.*

Sca1$^+$ cells are present in intimal lesions from murine carotid arteries following iatrogenic flow restriction (Sca1-eGFP mice)

The contribution of Sca1$^+$ cells to intimal medial thickening following iatrogenic flow restriction was assessed in Sca1-eGFP transgenic mice following partial ligation of the left carotid artery (LCA). Vessels were harvested on day 3, 7 and 14 d post-ligation and paraformaldehyde fixed and paraffin-embedded cross sections were evaluated for eGFP (indicative of Sca1 expression) by confocal microscopy. Morphometric analysis confirmed that following ligation injury the adventitial and intimal volumes increased significantly over time, without any significant change to medial volume, concomitant with a significant reduction in luminal volume after 7 and 14 days [Suppl Figure 2].

A small but significant number of Sca1-eGFP cells were present within the adventitial and intimal layers of the control (untouched) and sham operated (Sham) LCA [Figure 1(A, E)]. No Sca1-eGFP cells were visible within the medial layer of these vessels which consisted of α-smooth muscle actin (SMA)$^+$ cells [Figure 1A]. While the number of cells within the adventitial, medial and intimal layers of the LCA did not significantly change [Suppl Figure 3A], there was a significant increase in the fraction of Sca1-eGFP$^+$ cells within the intimal layer 3 d post ligation [Figure 1(B, E)]. Immunohistochemical analysis using anti-eGFP confirmed the presence of Sca1-eGFP cells [Figure 1C] and further demonstrated that intimal Sca1-GFP$^+$ cells co-express PECAM-1/CD31 and endothelial cell nitric oxide (eNOS) [Figure 1 (C, D)].

The effects of blood flow restriction on intimal thickening and the appearance of Sca1-eGFP cells was further assessed 7 and 14 days post ligation. The number and fraction of Sca1-eGFP cells present within the intimal layer increased over time post-ligation 7 and 14 days; [Suppl

Figure 3 (B,C), Figure 2(A-D)]. The majority of these cells were also SMA$^+$ positive [Suppl Figure 3D]. There was also a notable appearance of Sca1-eGFP cells within the medial layer of ligated LCA vessels [Figure 2 (A, B)]. These data confirm our previous studies that demonstrated chronic flow restriction promotes intimal thickening of the LCA concomitant with a significant increase in the number of Sca1$^+$ cells within the lesion (Fitzpatrick et al., 2017).

Flow restriction leading to changes in shear stress is associated with increased endothelial cell apoptosis *in vitro* (Pan et al., 2017) and *in vivo* (Heo et al., 2011). In order to address whether the increase in the fraction of intimal Sca1-eGFP cells was due to acute EC loss and subsequent cell turnover, the expression levels of the pro-apoptotic protein, Bax, as a surrogate marker for EC loss (Jagadeesha et al., 2009; Pawlowski and Kraft, 2000) was determined in the LCA and the contralateral right carotid artery (RCA) after 3 and 7 days [Figure 3]. There was a marked increase in Bax expression within intimal and medial cells of the LCA following acute ligation [Figure 3A], with a significant increase in the fraction of Bax positive cells after 3 days [Figure 3B]. By day 7, the fraction of Bax positive cells within both layers decreased [Figure 3(A, B)]. These data suggest that flow restriction promotes both intimal and medial cell apoptosis leading to EC and medial SMC cell loss. Endothelial regeneration was subsequently facilitated by the accumulation of intimal Sca1$^+$ cells.

S100β$^+$ cells are present in intimal lesions from murine carotid arteries following iatrogenic flow restriction (S100β-eGFP mice)

S100β$^+$ cells were assessed in carotids from S100β-eGFP transgenic mice following complete ligation of the LCA for 21 days. Morphometric analysis confirmed marked intimal thickening in the ligated carotids (LCA) when compared to the contralateral RCA and the sham LCA, respectively [Suppl Figure 4(A-C)]. A discrete number of perivascular S100β-eGFP cells were present in the adventitial layer of the RCA and the sham LCA [Figure 4 (A-C, G)], while none were detected in the medial or intimal layers. In ligated vessels, the number of S100β-eGFP cells significantly increased within the adventitial, medial, and intimal layers compared to sham controls and the contralateral RCA, respectively [Figure 4 (D-F, H)]. S100β-eGFP$^+$ cells were also evaluated for co-expression with Sca1$^+$ cells by immunohistochemistry using anti-Sca1

antibody. There was a significant increase in the number of S100β$^+$ cells that were also Sca1$^+$ in the media and intima of LCA when compared to RCA [Figure 5 (A-C)]. Collectively, these data suggest that intimal thickening results in the accumulation of medial and intimal cells that constitutively express both Sca1$^+$ and S100β$^+$

Hedgehog signalling components control intimal thickening following flow restriction

We previously reported that Hh signalling components are present in remodelled vessels and that local perivascular knockdown of the Ptch1 receptor ameliorated intimal thickening following ligation injury (Morrow et al., 2009; Redmond et al., 2013). Herein, we examined the effect of systemic administration of the Hedgehog inhibitor cyclopamine (10 mg/kg, IP, every other day). 2-hydroxypropyl-β-cyclodextrin (HβCD) was used as a vehicle control. Vessels were harvested 7 and 14 d post-ligation and morphometric analysis was performed. Whole vessel Gli2 mRNA levels were significantly elevated in ligated vessels treated with HβCD when compared to sham controls (8.1 ± 0.9 fold, $p \leq 0.05$ n=4), an effect that was significantly reduced following cyclopamine treatment (3.2 ± 0.3 fold, n=4, $p \leq 0.05$). Immunohistochemical analysis demonstrated that the Hh receptor, Ptch1, was up-regulated in LCA following injury concomitant with enhanced Gli2 expression in LCA when compared to sham vessels [Figure 6A]. Gli2 co-localised with Sca1$^+$-eGFP expressing cells and was markedly increased in ligated vessels treated with vehicle (HβCD) when compared to control sham-operated vessels, especially in the neointima and media of the LCA [Figure 6A]. Cyclopamine treatment significantly reduced the fraction of Gli2/Sca1$^+$-eGFP expressing cells [Figure 6(A-C)] concomitant with reduced intimal thickening 7 d- [Figure 6(D, F)] and 14 d-post ligation [Figure 6(E, G)]. Collectively, these data suggest that intimal thickening is attenuated by systemic administration of a smoothened inhibitor, cyclopamine, concomitant with a reduction in the accumulation of Gli2/Sca1$^+$ Hh-responsive cells within the intimal and medial layers.

Lineage tracing analysis of marked perivascular S100β cells following ligation injury

In order to determine the source of medial and intimal Sca1$^{+/}$S100β^{+} cells following ligation injury-induced remodeling, lineage tracing analysis was performed using transgenic *S100β-eGFP-CreERT2-Rosa-26-tdTomato* reporter mice [Suppl Figure 5A]. As cre-mediated recombination results in a permanent heritable change in a cell's genome, these cells and their progeny remain tdTomato (tdT^{+}) positive. The animals were treated with tamoxifen (for 7 days) to induce nuclear translocation of CreER(Tm) and subsequent recombination to indelibly mark S100β cells with red fluorescent tdT seven days before ligation injury was performed [Suppl Figure 5B]. Only S100β cells present during the period of tamoxifen treatment and their subsequent progeny following injury are marked with tdT. Morphometric analysis of the *S100β-eGFP-creER2-Rosa26-tdT* mice confirmed significant intimal thickening in both male and female transgenic mice following ligation injury [Suppl Figure 5C].

The tissue specificity and recombination efficiency of the tamoxifen- (Tm) induced Cre activity was confirmed in bone-marrow smears and neuronal tissue from *S100β-eGFP-CreERT2-Rosa-26-tdTomato* mice. Treatment with Tm resulted in Cre-mediated recombination and expression of S100β- tdT in >90% of neuronal cells of the carotid sinus nerve (Hering's nerve) without any S100β-tdT^{+} cells observed in the bone marrow smears [Suppl Figure 5D]. The neuronal staining was confirmed by immunohistochemical analysis of S100β expression using both anti-S100β and anti-tdT antibodies, in addition to S100β-eGFP and S100β-tdT staining within these neuronal cells [Suppl Figure 5D].

Treatment of *S100β-eGFP-creER2-Rosa26-tdT* transgenic mice with tamoxifen indelibly marked S100β cells (S100β-tdT^{+}) within the adventitial layer of the sham LCA prior to flow restriction [Figure 7A]. No cells are marked when these double transgenic mice were treated with the vehicle control (corn oil) [Figure 7C]. Importantly, no S100β-tdT^{+} cells were observed in the intimal (EC) or medial (SMC) layers of these sham vessels following tamoxifen treatment [Figure 7A, C]. However, following ligation injury, there was a striking increase in the number of S100β-tdT marked cells within the medial and intimal layers of the ligated LCA, compared to sham controls [Figure 7(B-E)]. Cumulative analysis confirmed a significant increase in the fraction of S100β-tdT cells within the LCA medial and intimal layers, compared to sham [Figure

7F]. In order to rule out the possibility that Tm treatment continues to label a significant number of cells for weeks after last Tm treatment (Reinert et al., 2012), we confirmed that the fraction of S100β-tdT marked cells following Tm-induced nuclear translocation of CreER(Tm) and subsequent recombination remained significantly higher in the intima of LCA compared to the RCA four weeks after the last Tm injection [Suppl Figure 5E, F]. Moreover, the fraction of S100β-tdT marked cells within the LCA adventitial, medial and intimal layers of ligated vessels after one and four weeks from the last Tm injection was of a similar magnitude [Suppl Figure 5G].

When S100β-tdT marked cells were evaluated for co-expression of Sca1 by immunohistochemistry using anti-Sca1 and anti-tdT antibodies, there was a significantly increased number of $Sca1^+$/S100β-tdT^+ in all compartments of the LCA compared to the contralateral RCA [Figure 8(A, B)]. Moreover, the majority of $Sca1^+$ cells (white) within the ligated vessel were S100β-TdT^+ [Figure 8(A, C)]. Since intimal and medial cells are not marked with tdT prior to injury, these data suggest that intimal and medial cells are derived from a non-SMC $S100β^+$ parent population following flow restriction *in vivo.* Moreover, the majority of intimal $Sca1^+$ cells are derived from an $S100β^+$ parent population.

Isolation and characterisation of resident $S100β^+$/$Sca1^+$ vascular stem cells from murine aorta.

The level of S100β and Sox10 expression, both markers of resident vascular stem cells (Kennedy et al., 2014a; Tang et al., 2012), was first assessed in atheroprone aortic arch (AA) and atheroresistant thoracic/abdominal aorta (TA) regions, with or without the adventitia. There was significant enrichment of both S100β and Sox10 in the AA when compared to the TA [Figure 9(A, B)]. Moreover, the levels were significantly enriched within the adventitia since its removal resulted in a dramatic reduction in the expression of both transcripts [Figure 9(A, B]. Nevertheless, medial expression of both genes was still observed in the AA region. The expression of SMC differentiation markers Myh11 and Cnn1 was similarly enriched in medial segments from both AA and TA regions of the mouse aorta [Figure 9C].

Resident vascular stem cells (vSCs) were isolated from mouse aortic arch (AA) and thoracic aorta (TA) by enzymatic digestion and sequential plating, and were characterised by immunocytochemistry, flow cytometry, and gene expression for both stem cell markers and

SMC differentiation markers. Immunocytochemical analysis revealed that vSCs from both AA and TA regions were Sca1 positive and expressed neuroectodermal markers S100β, Sox10, Sox17, and Nestin but were negative for SMC differentiation markers Cnn1 and Myh11 [Figure 9 (D, E)]. Flow cytometric analysis confirmed that the cells were Sca1 and S100β positive when compared to Sca1 and S100β positive control cell lines (i.e., C3H 10T1/2 and NE-4C, respectively) [Figure 9F].]. The vSCs did not enrich for Myh11 or Cnn1 transcripts when compared to fresh aortic tissue [Figure 9(G, H)] but exhibited greater teleomere length as a measure of stemness when compared to freshly isolated aortic SMC and to the immortalised MOVAS SMCs in culture [Figure 9I]. The vSCs were enriched for neuroectodermal marker genes S100β, Sox10 and Nestin [Figure 9 (J-L)], but not for mesoderm markers Kdr, Pax1 and Tbx6 [Figure 9 (M-O)], when compared to SMCs and NE-4 cells in culture. Collectively, these data indicate that neuroectodermal S100β$^+$/Sca1$^+$ cells are primarily located within the adventitial perivascular region of atheroprone regions of the mouse aorta and can be isolated and expanded *in vitro* to retain these phenotypic markers.

Hedgehog signalling promotes myogenic differentiation of resident murine S100β$^+$/Sca1$^+$ vascular stem cells.

The functional effect of sonic hedgehog (SHh) signalling on myogenic differentiation of vSCs was evaluated *in vitro* using multipotent Sca1$^+$/S100β$^+$ cells isolated from (i) mouse aorta, (ii) mouse embryonic stem cells (mESC), and (iii) rat adventitial progenitors. Treatment of vSCs isolated from AA and TA with recombinant SHh (rSHh, 0.5 µg/ml, 24h) promoted Hh signalling by increasing Gli1 target gene mRNA levels, an effect blocked following pre-treatment with the SMO inhibitor, cyclopamine [Figure 10(A, B)]. Concurrent treatment of cells with rSHh for 7 days resulted in a significant increase in SMC differentiation marker (Cnn1 and Myh11) mRNA levels, an effect attenuated by cyclopamine [Figure 10 (A, B)]. Treatment also significantly increased the fraction of Cnn1$^+$ and Myh11$^+$ cells in AA vSCs, an effect attenuated by pre-treatment with cyclopamine [Figure 10(C, D)].

Vascular SMCs maintain their SMC-specific epigenetic mark, di-methylation of lysine 4 on histone H3 (H3K4me2) at the Myh11 locus following de-differentiation *in vitro* (Gomez et al.,

2015; Majesky et al., 2017). Therefore, the level of enrichment of H3K4me2 and H3K27me3 (tri-methylation of lysine 27 on histone H3) at the Myh11 locus was assessed in mouse vSCs using chromatin immunoprecipitation (ChIP) assays before and after rSHh treatment. Freshly isolated differentiated aortic SMC and murine embryonic stem cells (mESCs) were used as positive/negative controls for each mark and were markedly enriched for H3K4me2 and H3K27me3 at the Myh11 promoter, respectively [Figure 10(E-G)]. In contrast to SMCs, murine AA vSCs were enriched for H3K27me3 but lacked enrichment of H3K4me2 at this locus [Figure 10E]. Moreover, treatment with recombinant SHh (rSHh, 0.5 μg/ml, 7d) increased the enrichment levels of the H3K4me2 histone mark while concurrently decreasing the enrichment of the repressor mark, H3K27me3 mark, an effect attenuated by cyclopamine [Figure 10(F, G)]. Collectively, these data suggest that Hh promotes myogenic differentiation of murine S100β$^+$/Sca1$^+$ vSCs *in vitro.* Importantly, these cells are not derived from medial SMCs as they are not marked by S100β-Cre *in vivo* nor do they express the stable H3K4me2 SMC epigenetic mark *in vitro.*

Sca1$^+$ progenitors were also isolated from mESCs and purified, as previously described (Tsai et al., 2012). These Sca1$^+$ cells are multipotent and capable of undergoing adipogenic and osteogenic differentiation [Suppl Figure 6(A-C)]. Using flow cytometry, Sca1$^+$-mESCs were negative for SMC differentiation markers, Myh11 and Cnn1, but positive for neuroectoderm markers Sox10, Sox17, and Pax6 when grown in their maintenance media [Suppl Figure 7A]. When stimulated with myogenic differentiation media supplemented with TGF-β1 (2 ng/ml) and PDGF-BB (10 ng/ml), Sca1$^+$-mESCs begin to undergo myogenic differentiation by increasing their expression of Myh11, and to a lesser extent Cnn1, while concomitantly maintaining their expression of Sox10, Sox17, and Pax6, and increasing their expression of S100β and Nestin [Suppl Figure 7A]. Immunoblot analysis confirmed the expression of neuroectoderm markers Sox10, Sox17, and to a lesser extent S100β, and the lack of expression of Myh11 and Cnn1 when Sca1$^+$ cells are grown in maintenance media. The cells undergo myogenic differentiation in response to TGF-β1/PDGF-BB as indicated by increased expression of SMA (α-actin), Cnn1 and Myh11 [Suppl Figure 7(A, C, D)] and decreased expression of Sca1 [Suppl Figure 7E]. Flow cytometric analysis confirmed that SHh promotes the differentiation of Sca1 cells and loss of

Sca1 expression in a similar manner to differentiation media supplemented with TGF-β1/PDGF-BB [Suppl Figure 7E].

Adventitial Sca1$^+$ progenitor cells (rAPCs) were also isolated by explant from rat aorta, purified and cloned. They expressed the Ptch1 receptor [Suppl Figure 8A] and increased Gli1 expression following SHh stimulation [Suppl Figure 8B] but notably lacked the H3K4me2 SMC epigenetic mark at the Myh11 promoter [Suppl Figure 8C]. Sca1$^+$ APCs underwent myogenic differentiation *in vitro* following stimulation with rSHh by increasing Cnn1 mRNA and the fraction of Cnn1$^+$ and Myh11$^+$ cells, an effect blocked by cyclopamine [Suppl Figure 8(D, E)]. Collectively, these data indicate that resident rat adventitial Sca1$^+$ vSCs, while not derived from SMCs (as they lack the H3K4me2 SMC mark), undergo myogenic differentiation in response to Hh signalling *in vitro.*

Hedgehog signalling promotes myogenic differentiation of human induced pluripotent stem cell (HiPSC)-derived neuroectodermal S100β vascular stem cells *in vitro.*

To address whether human neuroectoderm S100β$^+$ progenitors (NEPs) respond to hSHh by undergoing myogenic differentiation, S100β$^+$ NEPs were isolated from human induced pluripotent stem cells (HiPSC) using a chemically defined protocol (Cheung et al., 2012). Human iPSCs enriched for Oct4 were treated with neuroectodermal inductive stimuli (FGF-2 and the selective inhibitor of ALK5, SB413642) for 7 days [Figure 11A]. These NEPs are enriched for S100β but not SMC differentiation markers CNN1 and MYH11 [Figure 11(A-D)]. Treatment of NEPs with myogenic media supplemented with TGF-β1/PDGF-BB significantly increases the fraction of CNN1$^+$ and MYH11$^+$ cells after a further 12 d in culture, while concomitantly decreasing the number of S100β$^+$ cells [Figure 11(A-D)]. The levels of *S100β, CNN1* and *MYH11* transcripts mirrored the changes in protein, and NEP-derived SMCs became significantly enriched for *CNN1* and *MYH11* following TGF-β1/PDGF-BB treatment as they diminish their expression of S100β [Figure 11(E-G)]. Treatment of NEPs with rSHh (1.0 μg/ml) for 12 d resulted in a significant increase in the number of CNN1 positive cells [Figure 11H], concomitant with an increase in *CNN1* and *MYH11* mRNA levels, an effect attenuated by cyclopamine [Figure 11(I. J)].

Hedgehog signalling components and S100β$^+$ cells populate human arteriosclerotic lesions.

The expression of S100β and the hedgehog receptor, PTCH1, was determined by immunofluorescence staining in normal and arteriosclerotic human aortic sections. Vascular smooth muscle **α**-actin (SMA$^+$) cells were abundantly expressed in the medial layers of both normal and arteriosclerotic vessels, in addition to discrete SMA staining within the vasa vasorum of the adventitial layer of normal vessels and intense staining within the intima of arteriosclerotic sections [Figure 12A]. The expression of S100β was confined to the adventitial layer of normal vessels but was significantly enhanced withinn the adventitial and intimal layers of arteriosclerotic sections [Figure 12B]. The expression of PTCH1 was confined to the adventitial layers of normal vessels but was expressed in the medial and intimal layers of arteriosclerotic sections [Figure 12C].

Discussion

A hallmark of vascular pathology are neointimal hyperplastic lesions enriched with 'SMC-like' cells (Shi et al., 2019). Endothelial dysfunction due to changes in blood flow and shear stress precedes the appearance of these lesions and is considered a pivotal event in the development of arteriosclerosis and subclinical atherosclerosis (Sakamoto et al., 2018). GWAS studies have linked exaggerated Hh signalling to SMC fate and atherosclerosis (Aravani et al., 2019). Here, transgenic mice and genetic lineage tracing approaches were used to delineate the involvement of vascular progenitor cells in neointima formation. Our findings indicate that intimal thickening involves significant accumulation of Hh-responsive perivascular S100β$^+$-derived Sca1$^+$/S100β$^+$ myogenic progeny. Elucidation of this new cellular S100β$^+$ source for generating SMCs following injury expands our current understanding of vascular pathology and may represent an important therapeutic strategy for combating subclinical atherosclerosis.

SMC-like cells within neointimal lesions reportedly are monoclonal/oligoclonal in origin and arise from the expansion of a pre-existing resident clonal population of cells (Basatemur et al., 2019; Gomez and Owens, 2016; Hoglund et al., 2010; Murry et al., 1997). Despite extensive research, their origin remains controversial (Nguyen et al., 2013). In particular, whether these clonal progeny are derived primarily from differentiated medial SMCs (Campbell and Campbell, 2012; Chappell et al., 2016; Dobnikar et al., 2018), endothelial cells (Cooley et al., 2014; Yuan et al., 2017), and/or resident vSCs (Baker and Péault, 2016; Tang et al., 2020, 2012; Yuan et al., 2017; Zhang et al., 2018) remains unclear. Over the last decade, vascular SMC lineage tracing studies have provided compelling evidence of a putative role for pre-existing medial SMCs in vascular pathologies (Chappell et al., 2016; Herring et al., 2014; Nemenoff et al., 2011; Shankman et al., 2015). Single cell RNA sequence analysis (scRNA-seq) further identified a Sca1$^+$ Myh11-Cre marked SMC subpopulation that give rise to functionally distinct neointimal cells during lesion progression in mice (Chappell et al., 2016; Dobnikar et al., 2018). However, although the Myh11-CreERT2 transgene was originally deemed specific for vascular SMC (Owens, 2007), data indicating expression of this and other 'SMC differentiation genes' in non-SMC populations has recently emerged raising the possibility that other resident cells may contribute to lesion formation (Chakraborty et al., 2019; Murgai et al., 2017; Sheikh et al., 2014).

Myh11-CreER SMC lineage tracing studies have also demonstrated that the fraction of SMCs originating from pre-existing SMCs is considerably smaller after severe transmural injury in mice suggesting a contributory role for cells other than medial SMCs (Roostalu et al., 2018). As a general rule, SMCs are purported to switch from a contractile phenotype to a less mature synthetic phenotype following vascular injury (Campbell and Campbell, 2012). This phenotypic switch is accompanied by loss of expression of SMC differentiation contractile markers, increased proliferation, and the synthesis and release of several signalling molecules including pro-inflammatory cytokines, chemotaxis-associated molecules, and growth factors (Campbell and Campbell, 2012). In this study, we provide compelling genetic evidence that vascular lesions following ligation injury also contain an abundance of dual S100β$^+$/Sca1$^+$ cells derived from a non-SMC perivascular S100β$^+$ parent population. The reason for the apparent differences between our data and previous Myh11-CreER cell fate mapping studies is unclear, but may involve the use of tamoxifen (Tm) to induce nuclear translocation of CreER(Tm) and subsequent recombination in time-sensitive Tm-dependent Cre-LoxP models (Reinert et al., 2012). Tamoxifen (Tm) induced Cre recombinase has been shown to indelibly mark cells up to 4 weeks after the last Tm injection thereby potentially confounding the interpretation of many of these previous studies (Reinert et al., 2012). In this context, we found that the fraction of S100β-CreER (tdT$^+$) marked cells within the various compartments of ligated vessels four weeks after the last Tm injection was similar to that observed after one week, indicating that, at least in our hands, medial SMC that may undergo de-differentiation and acquire the S100β promoter are not being inadvertently marked after injury.

Notwithstanding the fact that Sca1$^+$ cells are present in bone-marrow (Tobin et al., 2017), Sca1$^+$ intimal cells are reportedly derived from a local source within the vessel wall (Hoglund et al., 2010). It is likely that the Sca1-eGFP cells observed in our study within intimal lesions are also locally derived. Adventitial Sca1$^+$ and c-kit$^+$ vSCs have long been implicated in the progression of neointimal lesions following various vascular injuries (Hu et al., 2004; Psaltis et al., 2014; Shikatani et al., 2016). However, in the absence of *in vivo* Sca1$^+$ or c-kit$^+$ stem cell lineage tracing experiments, the hypothesis of a regenerative function of Sca1$^+$ or c-kit$^+$ vSCs in lesion formation has been difficult to prove. Recent cell fate mapping studies have clarified a putative role for adventitial PDGFRa$^+$ Sca1$^+$ progenitors in SMC accumulation and vascular lesion

progression following severe transmural injury (but not wire-induced injury) (Tang et al., 2020) while c-kit$^+$ progenitors minimally facilitate endothelial regeneration or SMC differentiation to SMCs (Chen et al., 2018). Using Sca1$^+$-eGFP transgenic mice, we provide direct evidence that Sca1$^+$ cells are present within the medial and intimal layers of vascular lesions following flow restriction. Moreover, the source of these Sca1$^+$ cells in advanced lesions is an S100β$^+$ parent population as the Sca1$^+$ cells co-localised with S100β-CreER marked cells within these lesions. The Sca1$^+$/S100β$^+$ cells are predominantly found in the developing intimal layer after 7, 14 and 21 days, but some are also present in the medial layer. As previous studies have demonstrated significant apoptosis in medial SMCs following flow restriction (Skelly et al., 2007), the appearance of medial Sca1$^+$/S100β$^+$ cells is not surprising and may represent regeneration of medial SMCs following apoptosis and cell loss. While it is also possible that these medial Sca1$^+$/S100β$^+$ cells are derived from a rare population of Myh11-CreER/Sca1$^+$ cells (Dobnikar et al., 2018), this appears unlikely since medial Sca1$^+$/S100β$^+$ cells were mapped to a S100β-CreER non-SMC parent population before ligation.

Following ligation injury the presence of Sca1$^+$/S100β$^+$ cells within the neointima was genetically mapped to a non-SMC S100β$^+$ parent population following flow restriction. Since Sca1-CreER lineage cells were not present in vascular lesions following wire-induced injury (Tang et al., 2020), it is unlikely that neointimal cells are derived from a Sca1$^+$ parent population despite expressing Sca1. Indeed, the percentage of perivascular S100β-CreER marked cells that were Sca1$^+$ in normal vessels was < 50% indicating that a Sca1- negative S100β$^+$ positive population might be responsible. In this context, S100β has been shown to maintain an intermediate state of Sca1$^+$ progenitor cells following injury-induced lesion formation (Wu et al., 2019). Alternatively, this residual Sca1$^+$ S100β$^-$, population of adventitial Sca1$^+$ cells might represent Sca1$^+$ cells derived from differentiated MYh11-CreER SMCs that expand in number following injury and contribute to adventitial remodelling (Majesky et al., 2017). Although our fate mapping study provides direct evidence of S100β-CreER$^+$ cell contribution to lesion formation, it does not rule out that other stem cell sources may also contribute. Indeed, previous studies have reported that Sox10-Cre$^+$ (Yuan et al., 2017), Gli1-CreER$^+$ (Kramann et al., 2016) and Nestin-Cre$^+$ (Wan et al., 2012) cells generate SMCs and contribute to the neointima after injury. It is possible that these marked cells and S100β-CreER$^+$ cells represent subpopulations of the

same parent population. In any case, it would be interesting to examine whether these cells respond differently to vascular injury and adopt distinct cell fates in future studies.

Previous lineage tracing studies have implicated endothelial cells (EC) that undergo endothelial-to-mesenchymal transition (EndMT) as contributing to neointimal formation during vein graft remodelling (Cooley et al., 2014; Yuan et al., 2017). EndMT promotes neointimal hyperplasia and induces atherogenic differentiation of EC (Moonen et al., 2015). In our study, cell fate mapping of S100β$^+$ perivascular cells did not mark EC prior to flow restriction suggesting that the S100β-CreER$^+$ cells within lesions do not originate from an EC parent population. These apparent differences could be due to the different models of vascular injury used in the various studies. Previous studies employed vein graft and atherosclerosis models for the study of EndMT (Souilhol et al., 2018) that involve different biomechanical stimuli and/or a different inflammatory environment compared to the flow restriction vascular injury model we used. As flow restriction leading to alterations in shear stress is strongly associated with increased endothelial cell apoptosis *in vitro* (Pan et al., 2017) and *in vivo* (Heo et al., 2011), it is not surprising that we observed significant EC apoptosis and cell loss after 3d of flow restriction. We demonstrate that the Sca1$^+$ cells within the early regenerated intima maintain a CD31$^+$ and eNOS$^+$ endothelial cell phenotype. They do not contribute to the accumulation of advanced neointimal S100β/Sca1$^+$ or SMA$^+$ cells, as Sca1$^+$ EC are not marked using S100β-CreERT. The origin of these Sca1$^+$ EC cells is likely to be a Sca1$^+$ parent since Sca1-CreER$^+$ marked cells within the intimal layer maintain a CDH5$^+$ endothelial cell fate following wire-induced injury (Tang et al., 2020).

Several GWAS studies have implicated *HHIPL1*, an uncharacterized gene at the chromosome 14q32 CAD locus (van der Harst and Verweij, 2018; Schunkert et al., 2011), and identified it as a secreted Hh signaling activator that modulates atherosclerosis-relevant vascular phenotypes (Aravani et al., 2019). Here, we provide direct evidence that Hh controls vascular stem cells during pathologic remodelling. Specifically, we show that Hh responsive S100β$^+$/Sca1$^+$ stem cells contribute to intimal thickening and the progression of adaptive lesions *in vivo* following ligation injury, and furthermore that Hh signalling directs murine/rat S100β$^+$ resident vSCs and human induced pluripotent stem cell (HiPSC)-derived S100β$^+$ neuroectoderm stem cells to undergo myogenic SMC differentiation *in vitro*. Several previous lines of evidence point to a

role for Hh signalling in vascular lesion formation (Ali et al., 2013; Aravani et al., 2019; Beckers et al., 2007; Dutzmann et al., 2017; Li et al., 2010; Morrow et al., 2009; Wang et al., 2010). Adventitial Sca1$^+$ vSCs that co-localise with SHh and its receptor, Ptch1 (Passman et al., 2008) contribute to intimal thickening *in vivo* (Dutzmann et al., 2017; Shikatani et al., 2016; Tsai et al., 2012). Moreover, while we have previously reported that local perivascular knockdown of the Ptch1 receptor attenuates intimal thickening (Redmond et al., 2013), the directionality of Hh signalling following Ptch1 knockdown remained unclear. We now demonstrate that systemic inhibition of Hh signalling, using a smoothened inhibitor, significantly decreases arterial Ptch1 and Gli expression concomitant with a reduction in Sca1$^+$ cells and lesion formation *in vivo*. Previous studies have also shown that the Hippo developmental signalling pathway regulates SMC proliferation during cardiovascular development (Wang et al., 2014) and Yes-Associated Protein (YAP) is required for incorporation and expansion of Sca1-derived neointimal cells following injury (Tang et al., 2020). Of interest, using genetic interaction analyses, the Hh pathway reportedly acts upstream of the Hippo pathway in regulating stem cell maintenance (Fernandez-L et al., 2009). Future studies that address the interactions between Hippo pathway and Hh may yield therapeutic strategies aimed at interfering with YAP activity through inhibition of hedgehog pathway, which downregulates the YAP protein (Felley-Bosco and Stahel, 2014) (Cotton et al., 2017).

As vascular SMCs within the medial layer of arteries have several distinct developmental origins, their heterogeneity may partially dictate the propensity for lesion formation at a particular site and influence the progress of neointimal thickening (Cheung et al., 2012) (Leroux-Berger et al., 2011) (Bennett et al., 2016). SMC-like cells populating the atheroprone aortic arch region are derived from the neural crest (Jiang et al., 2000), while SMCs residing in the more athero-resistant descending aorta are derived from somatic mesoderm (Wasteson et al., 2008). We found that S100β$^+$/Sca1$^+$ cells isolated from atheroprone regions of the mouse and rat aorta were phenotypically neuroectodermal and responded to SHh by undergoing myogenic differentiation *in vitro* to become SMC-like cells. While S100β-CreER marked cells are primarily adventitial prior to ligation, and removal of the adventitia significantly reduced the expression of vSC markers (S100β and Sox10), a medial location for these cells cannot be fully ruled out. In particular, these cells may represent a sparse population within the media. Indeed, such a rare

population of medial Myh11-CreER lineage cells that express Sca1 has recently been reported (Dobnikar et al., 2018) and a low number of medial SMCs partake in lesion formation following SMC de-differentiation in response to injury (Chappell et al., 2016; Jacobsen et al., 2017). It is generally thought difficult to isolate cells exclusively from the medial or adventitial layer without the possibility of contamination of cells from the other layer, especially in rodent vascular tissues. Nevertheless, S100β$^+$/Sca1$^+$ cells are routinely described as being isolated from murine aortic media whereby aortic segments are cleared of EC and adventitial cells by enzymatic digestion prior to sequential plating or explant culture (Kennedy et al., 2014b, 2014a; Mathieu et al., 2020; Tang et al., 2012). *In situ* histochemical analysis of aorta from a Sox10-Cre mouse confirms the presence of a rare Sox10$^+$ cell population with the media, in addition to the adventitia (Tang et al., 2013). A discrete population of immature medial cells expressing CD146 is also known to emerge during embryonic development and contribute to neointimal formation in response to injury (Roostalu et al., 2018). Whether these CD146 immature SMC progenitors are also S100β$^+$/Sca1$^+$ remains unclear although vSCs derived from rat and murine aortic explants are CD146$^+$ (Kennedy et al., 2014a; Tang et al., 2012).

Further strong evidence that S100β$^+$/Sca1$^+$ vSCs isolated from murine AA and TA regions are not derived from a Myh11$^+$ medial SMC population is provided by our epigenetic data that show these cells do not enrich for a specific SMC histone mark on the promoter of SMC differentiation genes (McDonald et al., 2006). A SMC-specific epigenetic repertoire of histone modifications is acquired during development, including H3K4me2 of SMC marker genes such as Myh11 (Gomez et al., 2015). Importantly, enrichment of H3K4me2 at these loci is restricted to SMCs and absent in non-SMCs but persists when SMCs undergo de-differentiation and phenotypic switching *in vitro* (McDonald et al., 2006), and *in vivo* following injury (Shankman et al., 2015), a process dependent on activation of the ESC pluripotency factor KLF4 both *in vivo* (Salmon et al., 2012) and *in vitro* (McDonald et al., 2006). We found that Hh responsive S100β$^+$/Sca1$^+$ vSCs isolated from murine AA and TA regions and rat adventitial Sca1$^+$ cells did not enrich for this SMC histone mark. Instead, these S100β/Sca1$^+$ vSCs cells were enriched for the repressor H3K27me3 mark, and only enrich for the H3K4me2 SMC epigenetic mark when they undergo myogenic differentiation, an effect attenuated by the Hh inhibitor, cylopamine. In the future, it will be important to determine whether medial S100β$^+$ vSCs differ from CD146$^+$ and Myh11-

CreER Sca1$^+$ in their propensity to modulate different phenotypes and undergo clonal expansion. Taken together, these data suggest that S100β/Sca1$^+$ vSCs from AA and TA aortic segments are primarily located with the adventitial and medial layers, but a rare population may reside within the medial layer in normal arteries. Irrespective of their origin, they do not originate from medial SMCs as they lack the SMC-specific histone H3K4me2 mark. Previous studies report that perivascular cells must traverse the internal and external elastic lamina to accumulate within the intima following injury (Wang et al., 2012). Data confirm that disruption of the elastic lamellae and flow-dependent enlargement of fenestrae facilitate such migration (Campbell and Roach; Guo et al., 2008; Wong and Langille, 1996).

Previous immunohistochemical analysis of human vessels suggests that Hh components are expressed in medial and intimal SMCs, and in the adventitia of human arteries (Dunaeva et al., 2015; Queiroz et al., 2012). Our data clearly implicate a role for Hh responsive S100β$^+$ cells in vascular lesion formation in mice, and potentially in humans since S100β$^+$ and PTCH1$^+$ cells are present in normal arterial tissue. Their location is primarily within the adventitial layer where the Hh receptor PTCH1 is also expressed. In arteriosclerotic lesions, S100β expression is exaggerated in intimal SMA$^+$ SMC cells with staining for PTCH1 present. Importantly, Hh promoted myogenic differentiation of S100β$^+$ human neuroectoderm progenitors (NEPs) derived from hiPSC *in vitro*. As these NEP-derived SMCs are considered crucial to the generation of SMC in vascular lesions within atheroprone regions of the murine vasculature (Cheung et al., 2012; Sinha et al., 2014), it is tempting to speculate that Hh responsive S100β-derived myogenic progeny also play a pivotal role in lesion formation in humans. Indeed, as S100β cells maintain an intermediate state of Sca1$^+$ progenitors in mice (Wu et al., 2019), a similar scenario may pertain for a human Sca1-like progenitor cell. Of note, Sca1-like cells are present within human vascular lesions (Torsney et al., 2007) and other tissues (Smits et al., 2009; Valente et al., 2014) despite the lack of a human Sca1 ortholog (Holmes and Stanford, 2007). Sca1 is a member of the Ly6/uPAR gene family that includes 35 well-characterized human members. While the mouse gene family is considerably larger with 61 genes, Ly6/uPAR family proteins possess a well-conserved motif at the amino-terminus and carboxyl-terminus and this epitope is targeted by many anti-Sca1 antibody resides within this shared domain (Loughner et al., 2016).

It is well-known that SMC-like cells within vascular lesions consist of heterogeneous populations, reflecting the variable phenotypes and functions of these cells (Dobnikar et al., 2018; Zhang et al., 2018). However, what proportion of lesional SMC-like cells are derived from resident stem cells remains controversial. Our findings provide direct evidence of a significant role for Hh-responsive perivascular/medial S100β$^+$ vSCs and their progeny in adaptive lesions. Therefore, we contend that the identification of a population of S100β$^+$/Sca1$^+$ cells within vascular lesions that are derived from a non-SMC S100β$^+$ parent population is novel and an important source for intimal thickening following injury. Furthermore, the role of Shh in mediating this process expands our understanding of the mechanisms contributing to the progression of vascular lesions. Moreover, while hedgehog signalling has previously been implicated in the development of vascular lesions (Redmond et al., 2013) through modulation of a differentiated SMC phenotype (Aravani et al., 2019), our study further suggests that Hh signalling also controls the myogenic differentiation and accumulation of resident vSCs within vascular lesions. While hedgehog signalling appears critical, further research is required to investigate the precise mechanisms driving migration, proliferation and differentiation of stem cells during lesion formation. It is possible that SMC-like cells within lesions comprise several different stages of the myogenic, osteogenic and myeloid differentiation of various stem cells and hence display a variety of divergent phenotypes. The elucidation of these mechanisms will provide vital information needed for the development of more efficient and novel therapies for vascular proliferative diseases. Our results provide a potential strategy for the treatment of atherosclerosis by combating perivascular derived cell migration of a S100β parent vSC population. As S100β is critical to maintaining an intermediate progenitor cell (Wu et al., 2019), the role of Hh responsive perivascular S100β progeny within these adaptive lesions represents an important therapeutic target for treating subclinical arteriosclerosis.

Methods

Tamoxifen-induced genetic lineage tracing

S100β-CreER-Rosa26tdT mice (average weight 20g, 6-8 wks old) were injected IP with tamoxifen (Tm) dissolved in corn oil at 75 mg/kg for 5 consecutive days. Carotid artery ligation (partial, or complete), or sham operation, was performed at 1 wk or 4 wks after the last injection of Tm. At the indicated time post-ligation or sham operation, anesthetized mice were perfusion fixed and carotid arteries harvested for analysis.

Histomorphometry

At specified times post-ligation, mice were anesthetized (ketamine/xylazine) and perfusion fixed with 4% paraformaldehyde in sodium phosphate buffer (pH 7.0). Fixed carotids were embedded in paraffin for sectioning. Starting at the carotid bifurcation landmark (single lumen) a series of cross-sections (10 x 5 μm) were made, every 200 μm through 2 mm length of carotid artery. Cross-sections were de-paraffinized, rehydrated in graded alcohols and stained with Verhoeff-Van Gieson stain for elastic laminae and imaged using a Nikon TE300 microscope equipped with a Spot RT digital camera (Diagnostic Instruments). Digitized images were analyzed using SPOT Advanced imaging software. Assuming a circular structure *in vivo*, the circumference of the lumen was used to calculate the lumen area, the intimal area was defined by the luminal surface and internal elastic lamina (IEL), the medial area was defined by the IEL and external elastic lamina (EEL), and the adventitial area was the area between the EEL and the outer edge, essentially as described by us previously (Fitzpatrick et al., 2017; Liu et al., 2011).

Haematoxylin and Eosin Staining of Tissue

For human artery cross sections, slides were placed in ice-cold acetone and held at -20°C for 15 min. They were then washed 3 x PBS before immersion in Harris Haematoxylin at room temperature for 8 min. Slides were processed by sequential washing – in distilled water for 5 min; 1 % acid alcohol for 30 sec; 0.1 % sodium bicarbonate for 1 min and 95 % ethanol. Slides were then washed in Eosin for 1 min, 75 % ethanol for 3 min, 95 % ethanol for 3 min and 100

% ethanol for 3 min before being submerged in Histoclear for 3 min and permanently mounted using 3 drops of DPX, cleaned with 100 % ethanol before analysis.

For murine vessels, paraffin rehydration was conducted at room temperature by immersing the slides in xylene for 20 minutes. The slides were then immersed in the following gradients of ethanol for 5 minutes respectively: 100 %, 90 %, 70 % and 50 % ethanol. The slides were then rinsed in distilled H_2O_2 before washing in 1x PBS for 10 minutes. The slides were stored in 1x PBS until ready when they were immersed in Harris Haematoxylin at room temperature for 8 min.

Whole mount histochemical analysis

Briefly, arteries harvested from transgenic mice were washed in PBS before transfer to 10 % neutral buffered formalin and incubated at 4 °C overnight. The tissue was rinsed 3 x PBS before mounting on histology slides using DAPI containing fluoroshield. The whole tissue was then imaged using a Nikon Eclipse TS100 inverted microscope, EXFO X-Cite™ 120 fluorescence system and assessed using SPOT imaging software.

Immunofluorescent Staining of tissues.

Immunostaining essentially as previously described (Fitzpatrick et al., 2017; Liu et al., 2011; Morrow et al., 2009). Carotid artery cryosections were air-dried for 1 h at room temperature, followed by incubation with blocking buffer (5% donkey serum, 0.1% Triton X-100 in PBS) for 30 minutes at room temperature and then incubated with primary antibody overnight at 4^0C in antibody solution (2.5% BSA, 0.3M Glycine and 1% Tween in DPBS). Murine and human arterial sections were stained with primary antibodies [Supplementary Table I]. Isotype IgG control and secondary antibody only controls were performed. For antigen retrieval, slides were brought to a boil in 10 mM sodium citrate (pH 6.0) then maintained at a sub-boiling temperature for 10 minutes. Slides were cooled on the bench-top for 30 minutes then washed in deionized water (3x5 min) each before being washed in PBS (3x5 min). The antigen retrieval protocol diminishes endogenous eGFP and Tdt tomato transgene signals. Therefore, those sections were co-stained with anti-eGFP antibody and anti-Td tomato antibody [Supplementary Table I].

For immunofluorescence staining, 5 consecutive images were obtained and processed using ImageJ software™ to analyze the collected images. Images were merged using the Image color-merge channels function. Merged signals and split channels were used to delineate the signals at single-cell resolution. Settings were fixed at the beginning of both acquisition and analysis steps and were unchanged. Brightness and contrast were lightly adjusted after merging.

Immunocytofluorescent staining of cells

Cells seeded onto UV sterilized coverslips were fixed with 3.7 % formaldehyde, (15 min, RT). If cells required permeabilization for the detection of intracellular antigens, cells were incubated in 0.025 % Triton X-100 PBS (room temp, 15 min). All coverslips were blocked (1 hr, RT) using 5 % BSA, 0.3 M Glycine, 1 % Tween PBS solution (1 hr, RT). Cells were incubated (how long?) with primary antibodies [Supplemental Table II], then washed twice with PBS to remove any unbound primary antibody before being incubated (1 hr, RT) with the recommended concentration of fluorochrome-conjugated secondary antibodies diluted in blocking buffer [Supplementary Table II]. Following 2x wash in PBS, cell nuclei were stained using DAPI: PBS (dilution 1:1000) (15 min, RT). For each primary and secondary antibody used, a secondary control and an IgG isotype control was performed to assess nonspecific binding. An Olympus CK30 microscope and FCell™ software was used to capture images. Images were analysed using ImageJ software as described above. Settings were fixed at the beginning of both acquisition and analysis steps and were unchanged. Brightness and contrast were lightly adjusted after merging.

Chromatin Immunoprecipitation

ChIP was performed on cultured cells as previously described with slight modifications(Gomez et al., 2013a). Cells at 70% confluency were fixed with 1% paraformaldehyde (10 min, RT). Cross-link was stopped by addition of 125 mM glycine for 10 min. The cross-linked chromatin was sonicated to shear chromatin into fragments of 200–600 base pairs. The sheared chromatin was immunoprecipitated with 2 µg tri-methyl-histone H3 (Lys27) and di-methyl-histone H3 (Lys4), while negative control was incubated with mouse IgG and input DNA without antibody using the CHIP—IT Express HT Kit from Active Motif (Cat no: 53018) according to the

manufacturer's instructions [Supplementary Table III]. A chromatin IP DNA Purification Kit (Cat No 58002 Active Motif) was used to purify the samples after CHIP before PCR was performed using Myh11 primers [5' -CCC TCC CTT TGC TAA ACA CA - 3' and 5' - CCA GAT CCT GGG TCC TTA CA – 3] as previously published (Gomez et al., 2013b). Sensimix SYBR® no-ROX Bioline Kit (QT650) was used to perform Real Time One-Step PCR according to the manufacturers' instructions. The antibodies used for ChIP are outlined in Supplemental Table I

Quantitative PCR

Total RNA was prepared from cultured cells using the ReliaPrep™ RNA Cell Miniprep System kit from Promega according to the manufacturer's protocol. Two micrograms of RNA was used for reverse transcription with Rotor-Gene SYBR Green RT-PCR (QIAGEN) or The SensiMix™ SYBR® No-ROX (BioLine) protocols for Real TimeOne-Step RT-PCR using the Real Time Rotor-GeneRG-3000™ light cycler from Corbett Research using primers listed in Supplementary Table IV.

Flow cytometry and analysis

Isolated cells were incubated with I fluorochrome-conjugated antibodies and control IgG's or (ii) the appropriate primary antibody with fluorochrome-conjugated secondary antibodies at a final concentration of 1µg per sample and incubated at 4°C for 30 minutes [Supplementary Table V]. Fluorescence labeled cells analysis was performed using a BD FACS Aria flow cytometry system (BD Biosciences), and data were analyzed with FlowJo™ software (Tree Star, Ashland, Ore) and De Novo software FCS Express 4 Flow Cytometry (Pasadena, CA).

Western blot analysis

Total protein (~40µg) was resolved with SDS-PAGE and transferred to nitrocellulose membranes. The membrane was probed with primary antibodies [Supplementary Table II] and secondary anti-rabbit- anti-mouse antibody, HRP conjugated A5278 (Sigma) and anti-rabbit antibody, HRP conjugated A0545 (Sigma). Detection was performed using TMB T0565 (Sigma).

Telomere Assay

The average telomere length in cells was measured using a ScienCell's Absolute Mouse Telomere Length Quantification qPCR Assay Kit (AMTLQ) according to the manufacturer's instructions. The telomere primer set recognizes and amplifies telomere sequences and is designed to directly measure the average telomere length of murine cells.

QUANTIFICATION AND STATISTICAL ANALYSIS

All data were determined from multiple individual biological samples and presented as mean values ± standard error of the mean (SEM). All *in vitro* experiments were performed in triplicate and repeated three times unless otherwise stated. All mice were randomly assigned to groups (including both male and female), and the analysis was performed blind by two groups. For statistical comparisons, all data was checked for normal gaussian distribution before parametric and non-parametric tests were performed. An unpaired two-sided Student's t-test was performed using GraphPad Prism software v8™ for comparing differences between two groups, and ANOVA test for over multiple comparisons. Significance was accepted when $p \leq 0.05$.

EXPERIMENTAL MODEL AND SUBJECT DETAILS

Mice Breeding and Genotyping

All procedures were approved by the University of Rochester Animal Care Committee in accordance with the guidelines of the National Institutes of Health for the Care and Use of Laboratory Animals. Sca1-eGFP transgenic mice were obtained from JAX labs; Stock #012643, strain name B6.Cg.Tg(Ly6a-EGFP)G5Dzk/j. These transgenic mice have an enhanced green fluorescent protein (eGFP) under the control of murine lymphocyte antigen 6 complex, locus A (Ly6a) promoter. Hemizygous Ly6a-GFP mice are viable, fertile, normal in size and do not display any gross physical or behavioural abnormalities (Ma et al., 2002).

S100β-EGFP/Cre/ERT2 transgenic mice (JAX Labs, stock #014160, strain name B6;DBA-Tg(S100 β-EGFP/cre/ERT2)22Amc/j) express the eGFPCreER^{T2} (Enhanced Green Fluorescent Protein and tamoxifen inducible cre recombinase/ESR1) fusion gene under the direction of the mouse S100β promoter. Ai9 mice (Jax Labs, stock #007909, strain name B6.Cg-Gt(ROSA)26Sor$^{tm9(CAG\text{-}tdTomato)Hze}$ /J) express robust tdTomato fluorescence following Cre-mediated LoxP recombination. For lineage tracing experiments S100β-eGFP/Cre/ERT2–dTomato double transgenic mice of both genders were generated by crossing S100β-eGFP/Cre-ERT2 mice with Ai9 reporter mice. The tdTomato transgene expression pattern corresponds to genomically marked S100β, and the eGFP transgene expression pattern corresponds to current expression of S100β. Genomic DNA for genotyping was prepared from mice tail and papered for genotyping by Proteinase K lysed, isopropanol precipitated and 70% ethanol washed. The number of animals be used were approved based on the experiments effects size. All male and female mice were included in the study, and the start point (0 week) for each experiment involves adult mice of 8 weeks old.

Carotid Artery Ligation

Ligation of the left common carotid artery was performed essentially as described previously (Fitzpatrick et al., 2017; Morrow et al., 2009, 2010) 1 and 4 weeks after Tm-induced cre-recombination, in male and female S100β-eGFP/Cre/ERT2–dTomato double transgenic mice. Prior to surgery mice received a single dose of Buprenorphine SR (sustained release) analgesia (0.5-1.0 mg/kg SQ) (and every 72 hrs thereafter as needed). The animal was clipped and the surgical site prepped using betadine solution and alcohol. A midline cervical incision was made. For partial carotid artery ligation, with the aid of a dissecting microscope, the left external and internal carotid arterial branches were isolated and ligated with 6-0 silk suture reducing left carotid blood flow to flow via the patent occipital artery. The neck incision (2 layers, muscle and skin) was sutured closed. Partial ligation of the left carotid artery in this manner resulted in a decrease (~80%) in blood flow, leaving an intact endothelial monolayer. Buprenorphine was administered at least once post-op 6-12 hrs. For complete ligation, the left common carotid was

isolated and ligated just beneath the bifurcation with 6-0 silk suture. In sham surgery group, carotid was similarly manipulated but not ligated. The neck incision (2 layers, muscle and skin) was sutured closed and the animal allowed recover under observation. After 3, 7, 14 and 21 days, mice were perfused with 4% PFA via the left ventricle for 10 min, and carotid arteries were harvested for analysis.

Cyclopamine treatment

Sca1-eGFP mice were treated with the smoothened inhibitor, cyclopamine, or the vehicle 2-hydropropyl-β-cyclodextrin (HβCD) (Sigma-Aldrich) alone as a control, (essentially as described by van den Brink (Van Den Brink et al., 2001). Mice were injected (250 µl max volume) intraperitoneally (IP) 1 day before ligation, then every other day after ligation at a dose of 10 mg/kg Cyclopamine (Sigma-Aldrich) dissolved in a solution of 45% (w/v) HβCD. There was no effect of cyclopamine treatment on mouse body weight, compared to the HβCD vehicle control group (data not shown).

Cell culture and harvesting

Murine aortic SMCs (MOVAS (ATCC® CRL-2797™) were cultured in Dulbeco's Modified Eagles growth medium (DMEM) supplemented with Fetal Bovine Serum (10%), L-glutamine (2 mM, Gibco) and Penicillin-Streptomycin (100U/mL, Gibco). Murine neuroectodermal stem cells (mNE-4Cs, ATCC® CRL-2925™) were grown in Eagle's Minimum Essential Medium supplemented with Fetal Bovine Serum (10%), L-glutamine (2 mM, Gibco) and Penicillin-Streptomycin (100U/mL, Gibco) using Poly-L-Lysine coated plates (15 µg/ml). Murine embryonic C3H 10T1/2 cells (ATCC® CRL-226™) were grown in Eagle's Basal medium supplemented with heat-inactivated fetal bovine serum to a final concentration of 10% and 2mM L-glutamine. Murine embryonic stem cells (mESCs) ES-D3 [D3] (ATCC® CRL-1934™) were maintained in culture in Mouse ES Cell Basal Medium (ATCC SCRR-2011) supplemented with 2-mercaptoethanol (0.1 mM) and 15% ES-Cell Qualified FBS (ATCC SCRR-30-2020) and a 1,000 U/mL mouse leukemia inhibitory factor (LIF) (Millipore Cat. No. ESG1107). Murine vSCs from AA and TA regions of the mouse aorta were grown in DMEM media supplemented with chick embryo extract (2%), FBS embryonic qualified (1%, ATCC), B-27 Supplement, serum free, N-2 Supplement (Cell Therapy Systems), recombinant mouse bFGF (0.02 µg/mL), 2-

Mercaptoethanol (50nM), retinoic acid (100 nM), Penicillin-Streptomycin (100U/mL, Gibco) (MM).

Isolation of S100β/Sca1$^+$ murine resident vascular stem cells (vSCs)

Using an optimised enzymatic cell dissociation technique protocol vSCs from both atheroprone (aortic arch - neuroectodermal, NE), and athero-resistant (thoracic aorta- paraxial mesodermal, PM) regions of the murine aorta were isolated using sequential seeding on adherent and non—adherent plates. Mouse thoracic aortas (4 at a time) were harvested and placed in cold Hank's solution for adipose tissue removal and lumen rinsing. The adventitia was enzymatically removed by incubation of the vessels in collagenase solution [i.e., MEM α nucleosides GlutaMAX™ (2 ml) containing Collagenase type 1A (0.7 mg/ml), soybean trypsin inhibitor (50 mg/ml), and bovine serum albumin (1 mg/ml)] for approx. 10-20 min at 37°C. Once the adventitia became lose, it was carefully removed as an intact layer using forceps under a dissecting microscope. The aorta was divided into aortic arch (AA) and thoracic aorta (TA) regions and cut into 1 mm pieces and digested with Elastase type III (Sigma) at 37°C. Dispersed cells were centrifuged and washed twice in warm maintenance medium (MM) (DMEM supplemented with 2% chick embryo extract, 1% FBS, 0.02 μg/ml, bFGF basic protein, B-27 Supplement, N-2 supplement, 1% Penicillin-Streptomycin, 50 nM 2-Mercaptoethanol and 100 nM retinoic acid) before seeding (1st seeding) on a 6-well non-adherent plate in MM. At 48 h, suspension cells were transferred (2nd seeding) to a fresh well of a CELLstart™ pre-coated 6-well plate in MM. MM was added to the remaining cells in the non-adherent surface. Cells were incubated at 37°C, 5% CO_2 for 1 week with minimal disturbance. The stem cells exhibited a uniform neural-like morphology in low density culture adopting a dendritic-like tree shape and retaining their morphological characteristics at low density throughout repeated passage. Cells were fed with MM every 2-3 days and passaged every 3-4 days or when ~70% confluent.

Isolation of rat adventitial S100β$^+$/Sca1$^+$ progenitor stem cells (APCs)

Rat S100β/Sca1$^+$ adventitial progenitors (APCs) were isolated from adventitial layer of aorta from Sprague Dawley rats (100-200g) as an outgrowth of adventitial tissue as previously described (Hu et al., 2004; Tsai et al., 2012). Rat APCs were enriched for Sca-1$^+$ cells by immunomagnetic separation using magnetically activated cell sorter microbeads coated with antibodies to Sca-1 (Miltenyi Biotec). Rat Sca1$^+$ APCs were grown in EMEM supplemented with 2 mM L-glutamine and 10 % ATCC ESC qualified FBS and 100 U/ml penicillin, and 100 mg/ml streptomycin (GIBCO).

Generation of murine S100β$^+$/Sca1$^+$ from mouse embryonic stem cell (mESCs)

S100β$^+$/Sca1$^+$ cells were derived from mouse ESCs (ES-D3 cell line, CRL-1934; ATCC) as described previously (Xiao et al., 2007). Briefly, ESCs were cultured in ESC growth medium containing DMEM (ATCC), supplemented with 10 ng/ml recombinant human leukemia inhibitory factor (LIF, Chemicon), 10% FBS (ATCC), 2 mM L-glutamine (Sigma), 0.1 mM 2-mercaptoethanol (Sigma), 100 U/ml penicillin, and 100 mg/ml streptomycin (GIBCO) and maintained on gelatin (Sigma)-coated plates with a 1:6 to 1:10 ratio every 2–4 days. (Sigma). Cells were fed with fresh ESC growth medium every day. To generate Sca1$^+$ cells, mESCs were cultured in ESC growth medium on type IV mouse collagen (Sigma)-coated flasks for 3–4 days, before they were detached were detached with a 0.05% trypsin-EDTA solution (GIBCO) and incubated with the antibody-conjugated/coated microbeads at 4°C with occasional agitation for 15 min. The bead-bound cells were then selected using a magnetic cell separator (Miltenyi Biotec). Sca1$^+$ cells were resuspended and cultured in fresh ESC growth medium. To obtain higher numbers of Sca1$^+$ cells, these cells were expanded in ESC culture medium and re-sorted with anti-Sca-1 microbeads.

Generation of human neuroectoderm progenitors (NEPs) from induced pluripotent stem cells (HiPSCs)

Human induced pluripotent stem cells (HiPSC) were obtained from HipSci (Cambridge, UK) and cultured per the manufacturer's instructions. Briefly, human dermal fibroblasts were isolated from excess skin of patients undergoing plastic surgery and reprogrammed as previously described (Vallier et al., 2009). HiPSCs were grown on plates pre-coated using Vitronectin (10 µg/ml) and maintained in complete Essential eight medium replacing 95% of the medium daily.

A ROCK inhibitor (10 μM) was added to optimise colony growth. Cells were sub-cultured with 0.05 mM EDTA for 4-8 min at room temperature until colonies displayed bright halos around the edges and small holes appeared throughout. Cells were frozen down in knock-out serum solution with 10% DMSO. HiPSCs at 70% confluency were routinely split at a ratio of 1:10 and cells were used between passage 20-40.

For neuroectoderm differentiation, cells were grown in chemically defined neuroectodermal medium (CDM) containing IMDM, F12 nutrient mix, chemically defined lipid concentrate, transferrin, monothioglycerol, penicillin-streptomycin and 0.5 g of PVA, and insulin, as previously described (Cheung et al., 2012). Neuroectoderm differentiation was initiated in CDM supplemented with FGF2 (12 ng/ml) and SB431542 (10 μM) for 7 days. Neuroectodermal (NE) progenitors were maintained in CDM-PVA supplemented with FGF2 (12 ng/ml) and SB431542 (10 μM) and sub-cultured using TrypLE™ for 3–5 min at 37°C in a 5% CO_2 incubator. NE progenitors were used between passage 1-10.

To initiate myogenic SMC differentiation, NEPs were subcultured in SMC differentiation medium containing CDM + PDGF-BB (10 ng/ml, PeproTech) + TGF-β1 (2 ng/ml, PeproTech) for 12 days. Neuroectoderm-derived SMCs (NE-SMC) were maintained in CDM supplemented with 10% FBS. After 12 d of PDGF-BB and TGF-β1 treatment, all cells appeared spindle-shaped. Complete medium was then changed to DMEM 10% FBS, 1% Penicillin streptomycin for expansion. Cells were frozen down using 90% (volume/volume) FBS + 10% (vol/vol) DMSO. The NE-SMC were used between passage 3-20.

Human tissue

Tissue sections from paired normal human aorta and arteriosclerotic vessels were obtained from Amsbio LLC, tissue repository.

Acknowledgments:

A. We thank Diana Scott for histological tissue processing, and Drs. Linda Callahan and Paivi Jordan for confocal microscope expertise.

B. This research was funded in part by Science Foundation Ireland grant SFI-11/PI/1128, Health Research Board (HRB) of Ireland grant HRA-POR-2015-1315, the European Union's INTERREG VA Programme, managed by the Special EU Programmes Body (SEUPB) to PAC, and NIH R21AA020365 and R21AA023213 to EMR, Irish Research Council (IRC) GOIPG/2014/43 (M.DiL) and GOIPG/2016/1529 (E.C), King Abdulla Scholarship IR15208 ID1066336148 to Y.G.

C. The authors declare no competing financial interests.

D. E.F., W.L., J-C.H, performed the animal experiments and M.DiL and SH performed the blind analysis of the images. E.F performed the human arteriosclerotic tissue analysis. E.F., M.DiL., R.H., D.B., E.C., performed the murine and rat cell culture experiments, D.B performed the HiPSCs cell work. EC performed the telomere assay and R.H.J, MdiL and Y.G., performed the ChIP analysis. E.M.R., C.L., and P.A.C drafted the manuscript, revised the manuscript and discussed the results. E.M.R., and P.A.C., designed and coordinated the experiments, interpreted the data, revised and confirmed the paper. All authors reviewed and confirmed the manuscript.

E. Correspondence to Paul A. Cahill (paul.cahill@dcu.ie) and Eileen M Redmond (Eileen_redmond@urmc.rochester.edu)

F. No datasets were generated or analysed during the current study.

Figure Legends

Figure 1. Expression of Sca1-eGFP in the carotid artery 3 days post partial ligation. **(A, B)** Verhoeff-Van Gieson stained sections and corresponding confocal fluorescence images of DAPI nuclei (blue), Sca1-eGFP (green) and immunofluorescence of α-actin (SMA) (red) expression in (A) sham-operated and (B) ligated LCA vessels. **(C, D)** Verhoeff-Van Gieson stained sections and corresponding confocal fluorescence images of DAPI nuclei (blue), immunofluorescence of (C) anti-eGFP (green) anti-CD31 (red) and (D) anti-eNOS (red) expression in ligated LCA vessels. Arrows highlight Sca1-eGFP expressing cells in the adventitia (A), media (M) and neointima (NI) and CD31 and eNOS in intima. (**E)** The fraction of $Sca1^+$ cells/high power field (hpf) in the adventitia, media, and intima of sham and ligated vessels after 3 days. Data are the mean ± SEM of 3- 5 sections, #p≤ 0.05 from a minimum of 4 animals per experimental group. Scale bar = 20μm.

Figure 2. Expression of Sca1-eGFP in the carotid artery 7 and 14 days post partial ligation. **(A, B)** Representative Verhoeff-Van Gieson stained sections and corresponding confocal fluorescence images of DAPI nuclei (blue) and Sca1-eGFP (green) expression in ligated left carotid arteries (LCA) after (A) 7 days and (B) 14 days. **(C, D)** The fraction of $Sca1^+$ cells/ high power field (hpf) in the adventitia, media, and intima of sham and ligated vessels after (C) 7 days and (D) 14 days. Data are the mean ± SEM of 10 - 15 sections, #p≤ 0.05 from a minimum of 4 animals per experimental group. Scale bar = 20μm**.**

Figure 3. Bax expression in the carotid artery following flow restriction after 3 and 7 days. (**A)** Representative immunofluorescence images for the pro-apoptotic marker, Bax, (red) in ligated left carotid artery (LCA) vessels and contralateral right carotid artery (RCA) after 3 and 7d. IgG was used as a control. (**B)** The number of Bax^+ cells/hpf in the adventitia, media, and intima of sham and ligated vessels after 3 and 7 d. Arrows highlight Bax expressing cells within the adventitia (A), media (M), and neointima (NI). Data are the mean ± SEM of 3-6 sections per experimental group from 3 animals. #p≤ 0.05. Scale bar = 20μm.

Figure 4. Expression of S100β-eGFP in the carotid artery 21 days post ligation. **(A-D)** Confocal fluorescence images of DAPI nuclei (blue) and S100β-eGFP (green) expression in (A, B) right contralateral carotid artery (RCA) and (C, D) left ligated carotid artery (LCA) from sham and

ligated vessels. Scale bar = 20μm (top panel), 50μm (bottom panel). **(E, F)** Confocal fluorescence images of DAPI nuclei (blue) and S100β-eGFP (green) expression in ligated LCA vessels. Arrows highlight S100β-eGFP expressing cells within the adventitia (A), media (M), and neointima (NI). Scale bar = 20μm. **(G, H)** Cumulative analysis of the fraction of S100β-eGFP cells in the adventitia (A), media (M), and neointima (NI) of RCA and LCA. Data are the mean ± SEM, n=15-20 sections from 5 animals, #p≤ 0.05 vs Sham.

Figure 5. Co-expression of S100β$^+$ cells and Sca1$^+$ cells within the carotid artery of S100β-eGFP animals following ligation. (**A)** Representative confocal fluorescence images of DAPI nuclei (blue), immunofluorescence of anti-eGFP (green) expression and anti-Sca1 (far red, white) in the RCA and LCA 21 days post-ligation. Data are from a minimum of 3 animals per experimental group. Scale bar = 20μm. **(B, C)** Cumulative analysis of the fraction of (B) S100β-eGFP cells and (C) double positive S100β/Sca1$^+$ cells within the adventitia (A), media (M), and neointima (NI) of contralateral RCA and ligated LCA. Data are the mean ± SEM of five sections from 3 animals #p≤ 0.05 vs Sham.

Figure 6. Inhibition of Hh signalling attenuates intimal thickening and Sca1$^+$ cell expansion following ligation injury. (**A)** Representative immunofluorescence images of Hh receptor patched 1 (Ptch1) (red), Hh target gene Gli2 (red), Sca1-eGFP (green) expression and merged (eGFP/Gli2/DAPI) in carotid artery cross sections from sham-operated, ligated vehicle control (HβCD), and ligated + cyclopamine (10 mg/kg, IP) treated mice after 14 days. Scale bar = top panel: 50μm, all other panels: 20μm. **(B, C)** Cumulative data showing the fraction of Sca1-eGFP cells within the adventitia (A), media (M), and neointima (NI) from sham-operated, ligated vehicle control (HβCD), and ligated + cyclopamine (Cyl) Sca1-eGFP mice after (B) 7 days and (C) 14 days. Data are the mean ± SEM of five sections per experimental group, #p≤ 0.05 vs ligated HβCD controls and are representative of a minimum of 4 animals per experimental group. **(D, E)** Representative H&E staining of carotid artery cross sections from sham, ligated control (HβCD vehicle), and ligated + cyclopamine (Cyl) treated animals after 7 d (D) and 14 d (E). Scale bar = 50 μm**. (F, G)** Vessel compartment volumes for ligated control (HβCD), and ligated + cyclopamine (Cyl) treated animals after (F) 7d and (G) 14 d. Data mean ± SEM of 7-12 sections analysed from 4 animals, #p≤ 0.05 vs ligated control (HβCD),

Figure 7. Lineage tracing analysis of S100β-Cre(ERT2)-tdT marked cells within the carotid artery following flow restriction for 21 days. **(A, B)** Representative confocal fluorescence images of DAPI nuclei (blue) and S100β-tdT$^+$ (red) cells in (A) sham and (B) ligated LCA. Representative images shown; minimum of 4 animals per experimental group. Scale bar = 50μm**. (C-E).** Representative confocal fluorescence images of DAPI nuclei (blue) and S100β-tdT$^+$ (red) cells in ligated LCA treated with corn oil (control) or tamoxifen for 7 days prior to washout for 1 week and ligation. Arrows highlight S100β-tdT$^+$ (red) expressing cells within the adventitia (A), media (M), and neointima (NI). Scale bar = 20μm. (**F)** Cumulative analysis of the fraction of S100β-tdT$^+$ cells within the adventitia (A), media (M), and neointima (NI) of sham and ligated LCA. Data are the mean ± SEM of 15-20 sections per experimental group, #p≤ 0.05 from 4 animals per group.

Figure 8. Sca1$^+$ cells within the carotid artery following flow restriction are derived from a parent S100β-tdT$^+$ population. (**A)** Representative confocal fluorescence images of DAPI nuclei (blue), immunofluorescence of anti-tdT (red) and anti-Sca1 (far red, white) expression in the RCA and LCA 21 days post ligation. Scale bar = 20μm. **(B)** Cumulative analysis of the fraction of S100β/Sca1 cells and (**C)** percent of S100β-tdT$^+$ cells that are Sca1$^+$ within the adventitia (A), media (M), and neointima (NI) of contralateral RCA and ligated LCA. Data are the mean ± SEM 10-15 sections from 3 animals per group, #p≤ 0.05 vs Sham.

Figure 9. Characterisation of resident S100β$^+$/Sca1$^+$ vascular stem cells from atheroprone and atheroresistant regions of the mouse aorta. **(A, B)** The level of enrichment of mRNA for neuroectodermal markers A S100β and B Sox10 within atheroprone AA (aortic arch) and atheroresistant TA (thoracic/descending aorta) regions of the mouse aorta in the absence or presence of the adventitial (Adv) layer. The housekeeping gene hypoxanthine guanine phosphoribosyltransferase (HPRT) was used as a control. Data are expressed as the Log2 fold change in mRNA levels relative to murine aortic SMCs in culture and are the mean ± SEM of three aortic specimens, #p≤ 0.05 vs MOVAS SMCs. (**C)** Relative levels of Myh11 and Cnn1 in AA and TA regions of the mouse aorta. Data are expressed as the Log2 fold change in mRNA levels relative to neural stem cells (NE-4C) in culture and are the mean ± SEM of three aortic specimens, #p≤ 0.05 vs NE-4C cells. **(D, E)** Representative immunocytochemical analysis of stem cell markers S100β, Nestin, Sox10, Sox17, Sca1 and SMC differentiation markers, Cnn1

and Myh11 in vSCs isolated and grown in maintenance media (MM) from (D) AA and **(**E) TA regions of the mouse aorta. Scale bar 20μm**. (F)** Flow cytometry analysis of vSCs isolated from AA and TA regions of the mouse aorta and grown in maintenance media for S100β (dark green) and Sca1 (light green) expression. NE-4C and CH3-10T1/2 cells were used as positive controls, respectively. Filled dark and light green curves represent negative control samples. (**G, H)** Relative levels of (G) Myh11 and (H) Cnn1 in vSCs isolated from AA and TA regions of the mouse aorta, compared to AA and TA aortic tissue. Data are expressed as the Log2 fold change in mRNA levels relative to neural stem cells (NE-4C) in culture and are the mean ± SEM of three independent cultures and three aortic specimens, #p≤ 0.05 vs NE-4C cells. **(I)** Absolute telomere length of vSCs compared to cultured MOVAS SMC and fresh aortic tissue. The telomere primer set recognizes and amplifies telomere sequences. The single copy reference (SCR) primer set recognizes and amplifies a 100 bp-long region on mouse chromosome 10, and serves as reference for data normalization. Data are expressed as absolute telomere length (kb) and are the mean ± SEM of three plates and aortic specimens, #p≤ 0.05 vs MOVAs SMCs. (**J-L**) Relative levels of neuroectoderm markers (S100β, Sox10 and Nestin) and **(M-O)** paraxial mesoderm markers (Kdr, Pax1 and Tbx6) in vSCs isolated from AA and TA regions of the mouse aorta. Data are expressed as the Log2 fold change in mRNA levels relative to C3H 10T1/2 cells or neural stem cells (NE-4C) in culture and are the mean ± SEM of 3 independent cultures, *p≤ 0.05 vs C3H 10T1/2 cells (J-L), #p≤ 0.05 vs NE-4C (M-O).

Figure 10. Recombinant sonic hedgehog (rSHh) promotes myogenic differentiation of vSCs *in vitro.* (**A, B)** Relative levels of Gli1, Myh11 and Cnn1 within vSCs isolated from AA and TA regions of the mouse aorta in the absence or presence of rSHh (0.5 μg/ml) with or without the smoothened inhibitor, cyclopamine (10μM). Data are expressed as the Log2 fold change in mRNA levels relative to vSCs alone (control) and are the mean ± SEM of three representative wells from two independent experiments, #p≤ 0.05 versus rSHh alone. **(C, D)** Representative (C) immunocytofluorescence staining and (D) the fraction of $Cnn1^+$ and $Myh11^+$ cells in the absence or presence of rSHh (0.5 μg/ml) with or without cyclopamine (15μM) for 7 days. Representative images shown, Scale bar = 50 μm. Cumulative data is the mean ± SEM, n=3, #p≤ 0.05 versus control, *p≤ 0.05 vs rSHh. (**E)** The level of enrichment of H3K4me2 at the Myh11 locus by ChIP assay in AA vSCs in the absence or presence of rSHh (0.5 μg/ml) with or

without cyclopamine (15μM) for 7 d. Fresh aortic tissue and mouse ECSs was used as positive and negative controls, respectively. **(F, G)** The ratio of (F) H3K4me2:H3K27me3 and (G) H3K27me3:H3K4me2 at the Myh11 locus in in AA vSCs in the absence or presence of rSHh (0.5 μg/ml) with or without cyclopamine (15μM) for 7 d. Data are the mean ± SEM, n=3, #p≤ 0.05 versus aorta/ESC, *p≤ 0.05 vs vSC, §p≤ 0.05 vs rSHh.

Figure 11. Recombinant sonic hedgehog (rSHh) promotes myogenic differentiation of human induced pluripotent stem cell (HiPSC)-derived S100β$^+$ neuroectoderm progenitors (NEPs) *in vitro.* **(A)** Phase contrast images, fluorescence staining of DAPI nuclei (blue) and immunoctytochemical analysis of the expression of OCT4 (green), S100β (green) in NEPs and CNN1 (green) and MYH11 (green) in NEP-derived SMCs. All cells were generated as described previously (Cheung et al., 2012). Scale bar = Right panels: 50μm, Left panels: 20μm. Data are representative of five images per experimental group from three independent cultures. **(B-D)** The fraction of B S100β+, C CNN1$^+$ and D MYH11$^+$ cells in HiPSCs, NEPs and NEP-SMCs. Data are mean ± SEM, n=3, #p≤ 0.05 versus HiPSCs. **(E-G)** Relative levels of S100β, CNN1 and MYH11 in HiPSCs, NEPs and NEP-SMCs, respectively. Data are expressed as the Log2 fold change in mRNA levels relative to HiPSCs in culture and are the mean ± SEM, n=3, #p≤ 0.05 versus HiPSCs. **(H)** Immunoctytochemical analysis of CNN1 (green) expression and DAPI (blue) staining in NEPs in the absence or presence of recombinant hSHh (1.0 μg/ml) for 12 d. Data are representative of five images per experimental group from two independent cultures. **(I, J)** Relative levels of I CNN1 and J MYH11 in NEPs in the absence or presence of hSHh (0.5μg/ml) with or without cyclopamine (15μM) for 12 d. Data are representative of three independent cultures, #p≤ 0.05 versus NEPs, *p≤ 0.05 vs hSHh.

Figure 12. Human arteriosclerotic lesions express S100β$^+$ cells. **(A-C)** Representative phase contrast photomicrographs, hematoxylin and eosin (H&E) staining, DAPI staining (blue) and immunocytochemical staining for A smooth muscle cell α-actin (SMA) (red), B S100β (red) and C PTCH1 as indicated in the adventitial A, medial (M), and intimal I sections of human normal and arteriosclerotic arteries. Scale bar =50μm. Data are representative of 3 sections from 3 patient cohorts.

Bibliography

Ali, H., Emoto, N., Yagi, K., Vignon-Zellweger, N., Nakayama, K., Hatakeyama, K., Asada, Y., Rikitake, Y., and Hirata, K.-I. (2013). Localization and characterization of a novel secreted protein, SCUBE2, in the development and progression of atherosclerosis. Kobe J. Med. Sci. *59*, E122-31.

Aravani, D., Morris, G.E., Jones, P.D., Tattersall, H.K., Karamanavi, E., Kaiser, M.A., Kostogrys, R.B., Ghaderi Najafabadi, M., Andrews, S.L., Nath, M., et al. (2019). *HHIPL1* , a Gene at the 14q32 Coronary Artery Disease Locus, Positively Regulates Hedgehog Signaling and Promotes Atherosclerosis. Circulation *140*, 500–513.

Baker, A.H., and Péault, B. (2016). A Gli(1)ttering Role for Perivascular Stem Cells in Blood Vessel Remodeling. Cell Stem Cell *19*, 563–565.

Basatemur, G.L., Jørgensen, H.F., Clarke, M.C.H., Bennett, M.R., and Mallat, Z. (2019). Vascular smooth muscle cells in atherosclerosis. Nat. Rev. Cardiol. *16*, 727–744.

Beckers, L., Heeneman, S., Wang, L., Burkly, L.C., Rousch, M.M.J., Davidson, N.O., Gijbels, M.J.J., de Winther, M.P.J., Daemen, M.J.A.P., and Lutgens, E. (2007). Disruption of hedgehog signalling in ApoE - /- mice reduces plasma lipid levels, but increases atherosclerosis due to enhanced lipid uptake by macrophages. J. Pathol. *212*, 420–428.

Bennett, M.R., Sinha, S., and Owens, G.K. (2016). Vascular Smooth Muscle Cells in Atherosclerosis. Circ. Res. *118*, 692–702.

Van Den Brink, G.R., Hardwick, J.C.H., Peppelenbosch, M.P., Van Deventer, S.J.H., Tytgat, G.N.J., Brink, M.A., and Ten Kate, F.J. (2001). Sonic hedgehog regulates gastric gland morphogenesis in man and mouse. Gastroenterology *121*, 317–328.

Briscoe, J., and Thérond, P.P. (2013). The mechanisms of Hedgehog signalling and its roles in development and disease. Nat. Rev. Mol. Cell Biol. *14*, 416–429.

Campbell, G.J., and Roach, M.R. Fenestrations in the internal elastic lamina at bifurcations of human cerebral arteries. Stroke *12*, 489–496.

Campbell, J.H., and Campbell, G.R. (2012). Smooth Muscle Phenotypic Modulation—A Personal Experience. Arterioscler. Thromb. Vasc. Biol. *32*, 1784–1789.

Cao, T., Zhang, L., Yao, L.-L., Zheng, F., Wang, L., Yang, J.-Y., Guo, L.-Y., Li, X.-Y., Yan, Y.-W., Pan, Y.-M., et al. (2017). S100B promotes injury-induced vascular remodeling through modulating smooth muscle phenotype. Biochim. Biophys. Acta. Mol. Basis Dis. *1863*, 2772–2782.

Chakraborty, R., Saddouk, F.Z., Carrao, A.C., Krause, D.S., Greif, D.M., and Martin, K.A. (2019). Promoters to Study Vascular Smooth Muscle. Arterioscler. Thromb. Vasc. Biol. *39*, 603–612.

Chappell, J., Harman, J.L., Narasimhan, V.M., Yu, H., Foote, K., Simons, B.D., Bennett, M.R., and Jørgensen, H.F. (2016). Extensive Proliferation of a Subset of Differentiated, yet Plastic, Medial Vascular Smooth Muscle Cells Contributes to

Neointimal Formation in Mouse Injury and Atherosclerosis Models. Circ. Res. *119*, 1313–1323.

Chen, Q., Yang, M., Wu, H., Zhou, J., Wang, W., Zhang, H., Zhao, L., Zhu, J., Zhou, B., Xu, Q., et al. (2018). Genetic lineage tracing analysis of c-kit+ stem/progenitor cells revealed a contribution to vascular injury-induced neointimal lesions. J. Mol. Cell. Cardiol. *121*, 277–286.

Cheung, C., Bernardo, A.S., Trotter, M.W.B., Pedersen, R.A., and Sinha, S. (2012). Generation of human vascular smooth muscle subtypes provides insight into embryological origin-dependent disease susceptibility. Nat. Biotechnol. *30*, 165–173.

Cooley, B.C., Nevado, J., Mellad, J., Yang, D., St. Hilaire, C., Negro, A., Fang, F., Chen, G., San, H., Walts, A.D., et al. (2014). TGF- Signaling Mediates Endothelial-to-Mesenchymal Transition (EndMT) During Vein Graft Remodeling. Sci. Transl. Med. *6*, 227ra34-227ra34.

Cotton, J.L., Li, Q., Ma, L., Park, J.-S., Wang, J., Ou, J., Zhu, L.J., Ip, Y.T., Johnson, R.L., and Mao, J. (2017). YAP/TAZ and Hedgehog Coordinate Growth and Patterning in Gastrointestinal Mesenchyme. Dev. Cell *43*, 35-47.e4.

Dobnikar, L., Taylor, A.L., Chappell, J., Oldach, P., Harman, J.L., Oerton, E., Dzierzak, E., Bennett, M.R., Spivakov, M., and Jørgensen, H.F. (2018). Disease-relevant transcriptional signatures identified in individual smooth muscle cells from healthy mouse vessels. Nat. Commun. *9*, 4567.

Donato, R., Sorci, G., Riuzzi, F., Arcuri, C., Bianchi, R., Brozzi, F., Tubaro, C., and Giambanco, I. (2009). S100B's double life: intracellular regulator and extracellular signal. Biochim. Biophys. Acta *1793*, 1008–1022.

Dunaeva, M., van Oosterhoud, C., and Waltenberger, J. (2015). Expression of Hedgehog signaling molecules in human atherosclerotic lesions: An autopsy study. Int. J. Cardiol. *201*, 462–464.

Dutzmann, J., Koch, A., Weisheit, S., Sonnenschein, K., Korte, L., Haertlé, M., Thum, T., Bauersachs, J., Sedding, D.G., and Daniel, J.-M. (2017). Sonic hedgehog-dependent activation of adventitial fibroblasts promotes neointima formation. Cardiovasc. Res. *113*, 1653–1663.

Felley-Bosco, E., and Stahel, R. (2014). Hippo/YAP pathway for targeted therapy. Transl. Lung Cancer Res. *3*, 75–83.

Fernandez-L, A., Northcott, P.A., Dalton, J., Fraga, C., Ellison, D., Angers, S., Taylor, M.D., and Kenney, A.M. (2009). YAP1 is amplified and up-regulated in hedgehog-associated medulloblastomas and mediates Sonic hedgehog-driven neural precursor proliferation. Genes Dev. *23*, 2729–2741.

Fitzpatrick, E., Han, X., Liu, W., Corcoran, E., Burtenshaw, D., Morrow, D., Helt, J.-C., Cahill, P.A., and Redmond, E.M. (2017). Alcohol Reduces Arterial Remodeling by Inhibiting Sonic Hedgehog-Stimulated Stem Cell Antigen-1 Positive Progenitor Stem Cell Expansion. Alcohol. Clin. Exp. Res. *41*, 2051–2065.

Gomez, D., and Owens, G.K. (2016). Reconciling Smooth Muscle Cell Oligoclonality and Proliferative Capacity in Experimental Atherosclerosis. Circ. Res. *119*, 1262–

1264.

Gomez, D., Shankman, L.S., Nguyen, A.T., and Owens, G.K. (2013a). Detection of histone modifications at specific gene loci in single cells in histological sections. Nat. Methods *10*, 171–177.

Gomez, D., Shankman, L.S., Nguyen, A.T., and Owens, G.K. (2013b). Detection of histone modifications at specific gene loci in single cells in histological sections. Nat. Methods *10*, 171–177.

Gomez, D., Swiatlowska, P., and Owens, G.K. (2015). Epigenetic Control of Smooth Muscle Cell Identity and Lineage Memory. Arterioscler. Thromb. Vasc. Biol. *35*, 2508–2516.

Guo, Z.-Y., Yan, Z.-Q., Bai, L., Zhang, M.-L., and Jiang, Z.-L. (2008). Flow shear stress affects macromolecular accumulation through modulation of internal elastic lamina fenestrae. Clin. Biomech. *23*, S104–S111.

Halcox, J.P.J., Donald, A.E., Ellins, E., Witte, D.R., Shipley, M.J., Brunner, E.J., Marmot, M.G., and Deanfield, J.E. (2009). Endothelial Function Predicts Progression of Carotid Intima-Media Thickness. Circulation *119*, 1005–1012.

van der Harst, P., and Verweij, N. (2018). Identification of 64 Novel Genetic Loci Provides an Expanded View on the Genetic Architecture of Coronary Artery Disease. Circ. Res. *122*, 433–443.

Hayashi, A., Koob, J.W., Liu, D.Z., Tong, A.Y., Hunter, D.A., Parsadanian, A., Mackinnon, S.E., and Myckatyn, T.M. (2007). A double-transgenic mouse used to track migrating Schwann cells and regenerating axons following engraftment of injured nerves. Exp. Neurol. *207*, 128–138.

Heo, K.-S., Lee, H., Nigro, P., Thomas, T., Le, N.-T., Chang, E., McClain, C., Reinhart-King, C.A., King, M.R., Berk, B.C., et al. (2011). PKCζ mediates disturbed flow-induced endothelial apoptosis via p53 SUMOylation. J. Cell Biol. *193*, 867–884.

Herring, B., Hoggatt, A.M., Burlak, C., and Offermanns, S. (2014). Previously differentiated medial vascular smooth muscle cells contribute to neointima formation following vascular injury. Vasc. Cell *6*, 21.

Hoglund, V.J., Dong, X.R., and Majesky, M.W. (2010). Neointima formation: a local affair. Arterioscler. Thromb. Vasc. Biol. *30*, 1877–1879.

Holmes, C., and Stanford, W.L. (2007). Concise review: stem cell antigen-1: expression, function, and enigma. Stem Cells *25*, 1339–1347.

Hromada, C., Mühleder, S., Grillari, J., Redl, H., and Holnthoner, W. (2017). Endothelial Extracellular Vesicles-Promises and Challenges. Front. Physiol. *8*, 275.

Hu, Y., Zhang, Z., Torsney, E., Afzal, A.R., Davison, F., Metzler, B., and Xu, Q. (2004). Abundant progenitor cells in the adventitia contribute to atherosclerosis of vein grafts in ApoE-deficient mice. J. Clin. Invest. *113*, 1258–1265.

Hyman, J.M., Firestone, A.J., Heine, V.M., Zhao, Y., Ocasio, C.A., Han, K., Sun, M., Rack, P.G., Sinha, S., Wu, J.J., et al. (2009). Small-molecule inhibitors reveal multiple strategies for Hedgehog pathway blockade. Proc. Natl. Acad. Sci. U. S. A. *106*,

14132–14137.

Jacobsen, K., Lund, M.B., Shim, J., Gunnersen, S., Füchtbauer, E.-M., Kjolby, M., Carramolino, L., and Bentzon, J.F. (2017). Diverse cellular architecture of atherosclerotic plaque derives from clonal expansion of a few medial SMCs. JCI Insight *2*.

Jagadeesha, D.K., Miller, F.J., Bhalla, R.C., and Bhalla, R.C. (2009). Inhibition of apoptotic signaling and neointimal hyperplasia by tempol and nitric oxide synthase following vascular injury. J. Vasc. Res. *46*, 109–118.

Jiang, X., Rowitch, D.H., Soriano, P., McMahon, A.P., and Sucov, H.M. (2000). Fate of the mammalian cardiac neural crest. Development *127*, 1607–1616.

Kennedy, E., Hakimjavadi, R., Greene, C., Mooney, C.J., Fitzpatrick, E., Collins, L.E., Loscher, C.E., Guha, S., Morrow, D., Redmond, E.M., et al. (2014a). Embryonic rat vascular smooth muscle cells revisited - a model for neonatal, neointimal SMC or differentiated vascular stem cells? Vasc. Cell *6*, 6.

Kennedy, E., Mooney, C.J., Hakimjavadi, R., Fitzpatrick, E., Guha, S., Collins, L.E., Loscher, C.E., Morrow, D., Redmond, E.M., and Cahill, P.A. (2014b). Adult vascular smooth muscle cells in culture express neural stem cell markers typical of resident multipotent vascular stem cells. Cell Tissue Res. *358*, 203–216.

Korshunov, V.A., and Berk, B.C. (2003). Flow-induced vascular remodeling in the mouse: a model for carotid intima-media thickening. Arterioscler. Thromb. Vasc. Biol. *23*, 2185–2191.

Kramann, R., Goettsch, C., Wongboonsin, J., Iwata, H., Schneider, R.K., Kuppe, C., Kaesler, N., Chang-Panesso, M., Machado, F.G., Gratwohl, S., et al. (2016). Adventitial MSC-like Cells Are Progenitors of Vascular Smooth Muscle Cells and Drive Vascular Calcification in Chronic Kidney Disease. Cell Stem Cell *19*, 628–642.

Leroux-Berger, M., Queguiner, I., Maciel, T.T., Ho, A., Relaix, F., and Kempf, H. (2011). Pathologic calcification of adult vascular smooth muscle cells differs on their crest or mesodermal embryonic origin. J. Bone Miner. Res. *26*, 1543–1553.

Li, F., Duman-Scheel, M., Yang, D., Du, W., Zhang, J., Zhao, C., Qin, L., and Xin, S. (2010). Sonic hedgehog signaling induces vascular smooth muscle cell proliferation via induction of the G1 cyclin-retinoblastoma axis. Arterioscler. Thromb. Vasc. Biol. *30*, 1787–1794.

Liu, W., Redmond, E.M., Morrow, D., and Cullen, J.P. (2011). Differential effects of daily-moderate versus weekend-binge alcohol consumption on atherosclerotic plaque development in mice. Atherosclerosis *219*, 448–454.

López-Mejías, R., Corrales, A., Vicente, E., Robustillo-Villarino, M., González-Juanatey, C., Llorca, J., Genre, F., Remuzgo-Martínez, S., Dierssen-Sotos, T., Miranda-Filloy, J.A., et al. (2017). Influence of coronary artery disease and subclinical atherosclerosis related polymorphisms on the risk of atherosclerosis in rheumatoid arthritis. Sci. Rep. *7*, 40303.

Loughner, C.L., Bruford, E.A., McAndrews, M.S., Delp, E.E., Swamynathan, S., and Swamynathan, S.K. (2016). Organization, evolution and functions of the human and

mouse Ly6/uPAR family genes. Hum. Genomics *10*, 10.

Ma, X., Robin, C., Ottersbach, K., and Dzierzak, E. (2002). The *Ly‐6A* (Sca‐1) *GFP* Transgene is Expressed in all Adult Mouse Hematopoietic Stem Cells. Stem Cells *20*, 514–521.

Majesky, M.W., Horita, H., Ostriker, A., Lu, S., Regan, J.N., Bagchi, A., Dong, X.R., Poczobutt, J., Nemenoff, R.A., and Weiser-Evans, M.C.M. (2017). Differentiated Smooth Muscle Cells Generate a Subpopulation of Resident Vascular Progenitor Cells in the Adventitia Regulated by Klf4. Circ. Res. *120*, 296–311.

Mathieu, P.S., Fitzpatrick, E., Di Luca, M., Cahill, P.A., and Lally, C. (2020). Resident multipotent vascular stem cells exhibit amplitude dependent strain avoidance similar to that of vascular smooth muscle cells. Biochem. Biophys. Res. Commun. *521*, 762–768.

McDonald, O.G., Wamhoff, B.R., Hoofnagle, M.H., and Owens, G.K. (2006). Control of SRF binding to CArG box chromatin regulates smooth muscle gene expression in vivo. J. Clin. Invest. *116*, 36–48.

Moonen, J.-R.A.J., Lee, E.S., Schmidt, M., Maleszewska, M., Koerts, J.A., Brouwer, L.A., van Kooten, T.G., van Luyn, M.J.A., Zeebregts, C.J., Krenning, G., et al. (2015). Endothelial-to-mesenchymal transition contributes to fibro-proliferative vascular disease and is modulated by fluid shear stress. Cardiovasc. Res. *108*, 377–386.

Morrow, D., Cullen, J.P., Liu, W., Guha, S., Sweeney, C., Birney, Y.A., Collins, N., Walls, D., Redmond, E.M., and Cahill, P.A. (2009). Sonic Hedgehog induces Notch target gene expression in vascular smooth muscle cells via VEGF-A. Arterioscler. Thromb. Vasc. Biol. *29*, 1112–1118.

Morrow, D., Cullen, J.P., Liu, W., Cahill, P.A., and Redmond, E.M. (2010). Alcohol inhibits smooth muscle cell proliferation via regulation of the Notch signaling pathway. Arterioscler. Thromb. Vasc. Biol. *30*, 2597–2603.

Murgai, M., Ju, W., Eason, M., Kline, J., Beury, D.W., Kaczanowska, S., Miettinen, M.M., Kruhlak, M., Lei, H., Shern, J.F., et al. (2017). KLF4-dependent perivascular cell plasticity mediates pre-metastatic niche formation and metastasis. Nat. Med. *23*, 1176–1190.

Murry, C.E., Gipaya, C.T., Bartosek, T., Benditt, E.P., and Schwartz, S.M. (1997). Monoclonality of smooth muscle cells in human atherosclerosis. Am. J. Pathol. *151*, 697–705.

Nam, D., Ni, C.-W., Rezvan, A., Suo, J., Budzyn, K., Llanos, A., Harrison, D., Giddens, D., and Jo, H. (2009). Partial carotid ligation is a model of acutely induced disturbed flow, leading to rapid endothelial dysfunction and atherosclerosis. Am. J. Physiol. Heart Circ. Physiol. *297*, H1535-43.

Nemenoff, R.A., Horita, H., Ostriker, A.C., Furgeson, S.B., Simpson, P.A., VanPutten, V., Crossno, J., Offermanns, S., and Weiser-Evans, M.C.M. (2011). SDF-1α induction in mature smooth muscle cells by inactivation of PTEN is a critical mediator of exacerbated injury-induced neointima formation. Arterioscler. Thromb. Vasc. Biol. *31*, 1300–1308.

Nguyen, A.T., Gomez, D., Bell, R.D., Campbell, J.H., Clowes, A.W., Gabbiani, G., Giachelli, C.M., Parmacek, M.S., Raines, E.W., Rusch, N.J., et al. (2013). Smooth muscle cell plasticity: fact or fiction? Circ. Res. *112*, 17–22.

Owens, G.K. (2007). Molecular control of vascular smooth muscle cell differentiation and phenotypic plasticity. Novartis Found. Symp. *283*, 174–191; discussion 191-3, 238–241.

Pan, L., Hong, Z., Yu, L., Gao, Y., Zhang, R., Feng, H., Su, L., and Wang, G. (2017). Shear stress induces human aortic endothelial cell apoptosis via interleukin-1 receptor-associated kinase 2-induced endoplasmic reticulum stress. Mol. Med. Rep. *16*, 7205–7212.

Passman, J.N., Dong, X.R., Wu, S.-P., Maguire, C.T., Hogan, K.A., Bautch, V.L., and Majesky, M.W. (2008). A sonic hedgehog signaling domain in the arterial adventitia supports resident Sca1+ smooth muscle progenitor cells. Proc. Natl. Acad. Sci. U. S. A. *105*, 9349–9354.

Pawlowski, J., and Kraft, A.S. (2000). Bax-induced apoptotic cell death. Proc. Natl. Acad. Sci. U. S. A. *97*, 529–531.

Psaltis, P.J., Puranik, A.S., Spoon, D.B., Chue, C.D., Hoffman, S.J., Witt, T.A., Delacroix, S., Kleppe, L.S., Mueske, C.S., Pan, S., et al. (2014). Characterization of a resident population of adventitial macrophage progenitor cells in postnatal vasculature. Circ. Res. *115*, 364–375.

Queiroz, K.C.S., Bijlsma, M.F., Tio, R.A., Zeebregts, C.J., Dunaeva, M., Ferreira, C. V, Fuhler, G.M., Kuipers, E.J., Alves, M.M., Rezaee, F., et al. (2012). Dichotomy in Hedgehog signaling between human healthy vessel and atherosclerotic plaques. Mol. Med. *18*, 1122–1127.

Redmond, E.M., Hamm, K., Cullen, J.P., Hatch, E., Cahill, P.A., and Morrow, D. (2013). Inhibition of patched-1 prevents injury-induced neointimal hyperplasia. Arterioscler. Thromb. Vasc. Biol. *33*, 1960–1964.

Reinert, R.B., Kantz, J., Misfeldt, A.A., Poffenberger, G., Gannon, M., Brissova, M., and Powers, A.C. (2012). Tamoxifen-Induced Cre-loxP Recombination Is Prolonged in Pancreatic Islets of Adult Mice. PLoS One *7*, e33529.

Roostalu, U., Aldeiri, B., Albertini, A., Humphreys, N., Simonsen-Jackson, M., Wong, J.K.F., and Cossu, G. (2018). Distinct Cellular Mechanisms Underlie Smooth Muscle Turnover in Vascular Development and Repair. Circ. Res. *122*, 267–281.

Sagheddu, R., Chiappalupi, S., Salvadori, L., Riuzzi, F., Donato, R., and Sorci, G. (2018). Targeting RAGE as a potential therapeutic approach to Duchenne muscular dystrophy. Hum. Mol. Genet. *27*, 3734–3746.

Sakamoto, A., Torii, S., Jinnouchi, H., Finn, A. V, Virmani, R., and Kolodgie, F.D. (2018). Pathologic intimal thickening: Are we any closer to understand early transitional plaques that lead to symptomatic disease? Atherosclerosis *274*, 227–229.

Salmon, M., Gomez, D., Greene, E., Shankman, L., and Owens, G.K. (2012). Cooperative binding of KLF4, pELK-1, and HDAC2 to a G/C repressor element in the SM22α promoter mediates transcriptional silencing during SMC phenotypic switching

in vivo. Circ. Res. *111*, 685–696.

Schneider, R.K., Mullally, A., Dugourd, A., Peisker, F., Hoogenboezem, R., Van Strien, P.M.H., Bindels, E.M., Heckl, D., Büsche, G., Fleck, D., et al. (2018). Gli1+ Mesenchymal Stromal Cells Are a Key Driver of Bone Marrow Fibrosis and an Important Cellular Therapeutic Target. Cell Stem Cell *23*, 308–309.

Schunkert, H., König, I.R., Kathiresan, S., Reilly, M.P., Assimes, T.L., Holm, H., Preuss, M., Stewart, A.F.R., Barbalic, M., Gieger, C., et al. (2011). Large-scale association analysis identifies 13 new susceptibility loci for coronary artery disease. Nat. Genet. *43*, 333–338.

Seidelmann, S.B., Lighthouse, J.K., and Greif, D.M. (2014). Development and pathologies of the arterial wall. Cell. Mol. Life Sci. *71*, 1977–1999.

Shankman, L.S., Gomez, D., Cherepanova, O.A., Salmon, M., Alencar, G.F., Haskins, R.M., Swiatlowska, P., Newman, A.A.C., Greene, E.S., Straub, A.C., et al. (2015). KLF4-dependent phenotypic modulation of smooth muscle cells has a key role in atherosclerotic plaque pathogenesis. Nat. Med. *21*, 628–637.

Sheikh, A.Q., Lighthouse, J.K., and Greif, D.M. (2014). Recapitulation of Developing Artery Muscularization in Pulmonary Hypertension. Cell Rep. *6*, 809–817.

Shi, N., Mei, X., and Chen, S.-Y. (2019). Smooth Muscle Cells in Vascular Remodeling. Arterioscler. Thromb. Vasc. Biol. *39*.

Shikatani, E.A., Chandy, M., Besla, R., Li, C.C., Momen, A., El-Mounayri, O., Robbins, C.S., and Husain, M. (2016). c-Myb Regulates Proliferation and Differentiation of Adventitial Sca1+ Vascular Smooth Muscle Cell Progenitors by Transactivation of Myocardin. Arterioscler. Thromb. Vasc. Biol. *36*, 1367–1376.

Sinha, S., Iyer, D., and Granata, A. (2014). Embryonic origins of human vascular smooth muscle cells: implications for in vitro modeling and clinical application. Cell. Mol. Life Sci. *71*, 2271–2288.

Skelly, C.L., Chandiwal, A., Vosicky, J.E., Weichselbaum, R.R., and Roizman, B. (2007). Attenuated herpes simplex virus 1 blocks arterial apoptosis and intimal hyperplasia induced by balloon angioplasty and reduced blood flow.

Smits, A.M., van Vliet, P., Metz, C.H., Korfage, T., Sluijter, J.P., Doevendans, P.A., and Goumans, M.-J. (2009). Human cardiomyocyte progenitor cells differentiate into functional mature cardiomyocytes: an in vitro model for studying human cardiac physiology and pathophysiology. Nat. Protoc. *4*, 232–243.

Souilhol, C., Harmsen, M.C., Evans, P.C., and Krenning, G. (2018). Endothelial–mesenchymal transition in atherosclerosis. Cardiovasc. Res. *114*, 565–577.

Tang, J., Wang, H., Huang, X., Li, F., Zhu, H., Li, Y., He, L., Zhang, H., Pu, W., Liu, K., et al. (2020). Arterial Sca1+ Vascular Stem Cells Generate De Novo Smooth Muscle for Artery Repair and Regeneration. Cell Stem Cell *26*, 81-96.e4.

Tang, Z., Wang, A., Yuan, F., Yan, Z., Liu, B., Chu, J.S., Helms, J.A., and Li, S. (2012). Differentiation of multipotent vascular stem cells contributes to vascular diseases. Nat. Commun. *3*, 875.

Tang, Z., Wang, A., Wang, D., and Li, S. (2013). Smooth muscle cells: to be or not to be? Response to Nguyen et Al. Circ. Res. *112*, 23–26.

Tobin, S.W., Li, S.-H., Li, J., Wu, J., Yeganeh, A., Yu, P., Weisel, R.D., and Li, R.-K. (2017). Dual roles for bone marrow–derived Sca-1 cells in cardiac function. FASEB J. *31*, 2905–2915.

Torsney, E., Mandal, K., Halliday, A., Jahangiri, M., and Xu, Q. (2007). Characterisation of progenitor cells in human atherosclerotic vessels. Atherosclerosis *191*, 259–264.

Tsai, T.-N., Kirton, J.P., Campagnolo, P., Zhang, L., Xiao, Q., Zhang, Z., Wang, W., Hu, Y., and Xu, Q. (2012). Contribution of stem cells to neointimal formation of decellularized vessel grafts in a novel mouse model. Am. J. Pathol. *181*, 362–373.

Valente, M., Nascimento, D.S., Cumano, A., and Pinto-do-Ó, P. (2014). Sca-1+ cardiac progenitor cells and heart-making: a critical synopsis. Stem Cells Dev. *23*, 2263–2273.

Vallier, L., Touboul, T., Brown, S., Cho, C., Bilican, B., Alexander, M., Cedervall, J., Chandran, S., Ährlund-Richter, L., Weber, A., et al. (2009). Signaling Pathways Controlling Pluripotency and Early Cell Fate Decisions of Human Induced Pluripotent Stem Cells. Stem Cells *27*, 2655–2666.

Wan, M., Li, C., Zhen, G., Jiao, K., He, W., Jia, X., Wang, W., Shi, C., Xing, Q., Chen, Y.-F., et al. (2012). Injury-activated transforming growth factor β controls mobilization of mesenchymal stem cells for tissue remodeling. Stem Cells *30*, 2498–2511.

Wang, G., Zhang, Z., Xu, Z., Yin, H., Bai, L., Ma, Z., Decoster, M.A., Qian, G., and Wu, G. (2010). Activation of the sonic hedgehog signaling controls human pulmonary arterial smooth muscle cell proliferation in response to hypoxia. Biochim. Biophys. Acta *1803*, 1359–1367.

Wang, Y.-L., Liu, L.-Z., He, Z.-H., Ding, K.-H., and Xue, F. (2012). Phenotypic transformation and migration of adventitial cells following angioplasty. Exp. Ther. Med. *4*, 26–32.

Wang, Y., Hu, G., Liu, F., Wang, X., Wu, M., Schwarz, J.J., and Zhou, J. (2014). Deletion of yes-associated protein (YAP) specifically in cardiac and vascular smooth muscle cells reveals a crucial role for YAP in mouse cardiovascular development. Circ. Res. *114*, 957–965.

Wasteson, P., Johansson, B.R., Jukkola, T., Breuer, S., Akyurek, L.M., Partanen, J., and Lindahl, P. (2008). Developmental origin of smooth muscle cells in the descending aorta in mice. Development *135*, 1823–1832.

Wong, L.C.Y., and Langille, B.L. (1996). Developmental Remodeling of the Internal Elastic Lamina of Rabbit Arteries. Circ. Res. *78*, 799–805.

Wu, Y., Liu, X., Guo, L.-Y., Zhang, L., Zheng, F., Li, S., Li, X.-Y., Yuan, Y., Liu, Y., Yan, Y.-W., et al. (2019). S100B is required for maintaining an intermediate state with double-positive Sca-1+ progenitor and vascular smooth muscle cells during neointimal formation. Stem Cell Res. Ther. *10*, 294.

Xiao, Q., Zeng, L., Zhang, Z., Hu, Y., and Xu, Q. (2007). Stem cell-derived Sca-1+ progenitors differentiate into smooth muscle cells, which is mediated by collagen IV-integrin alpha1/beta1/alphav and PDGF receptor pathways. Am. J. Physiol. Cell Physiol. *292*, C342-52.

Yuan, F., Wang, D., Xu, K., Wang, J., Zhang, Z., Yang, L., Yang, G.-Y., and Li, S. (2017). Contribution of Vascular Cells to Neointimal Formation. PLoS One *12*, e0168914.

Zhang, C., Zeng, L., Emanueli, C., and Xu, Q. (2013). Blood flow and stem cells in vascular disease. Cardiovasc. Res. *99*, 251–259.

Zhang, L., Issa Bhaloo, S., Chen, T., Zhou, B., and Xu, Q. (2018). Role of Resident Stem Cells in Vessel Formation and Arteriosclerosis. Circ. Res. *122*, 1608–1624.

Zhou, S., Zhu, W., Zhang, Y., Pan, S., and Bao, J. (2018). S100B promotes microglia M1 polarization and migration to aggravate cerebral ischemia. Inflamm. Res. *67*, 937–949.

Figure 1

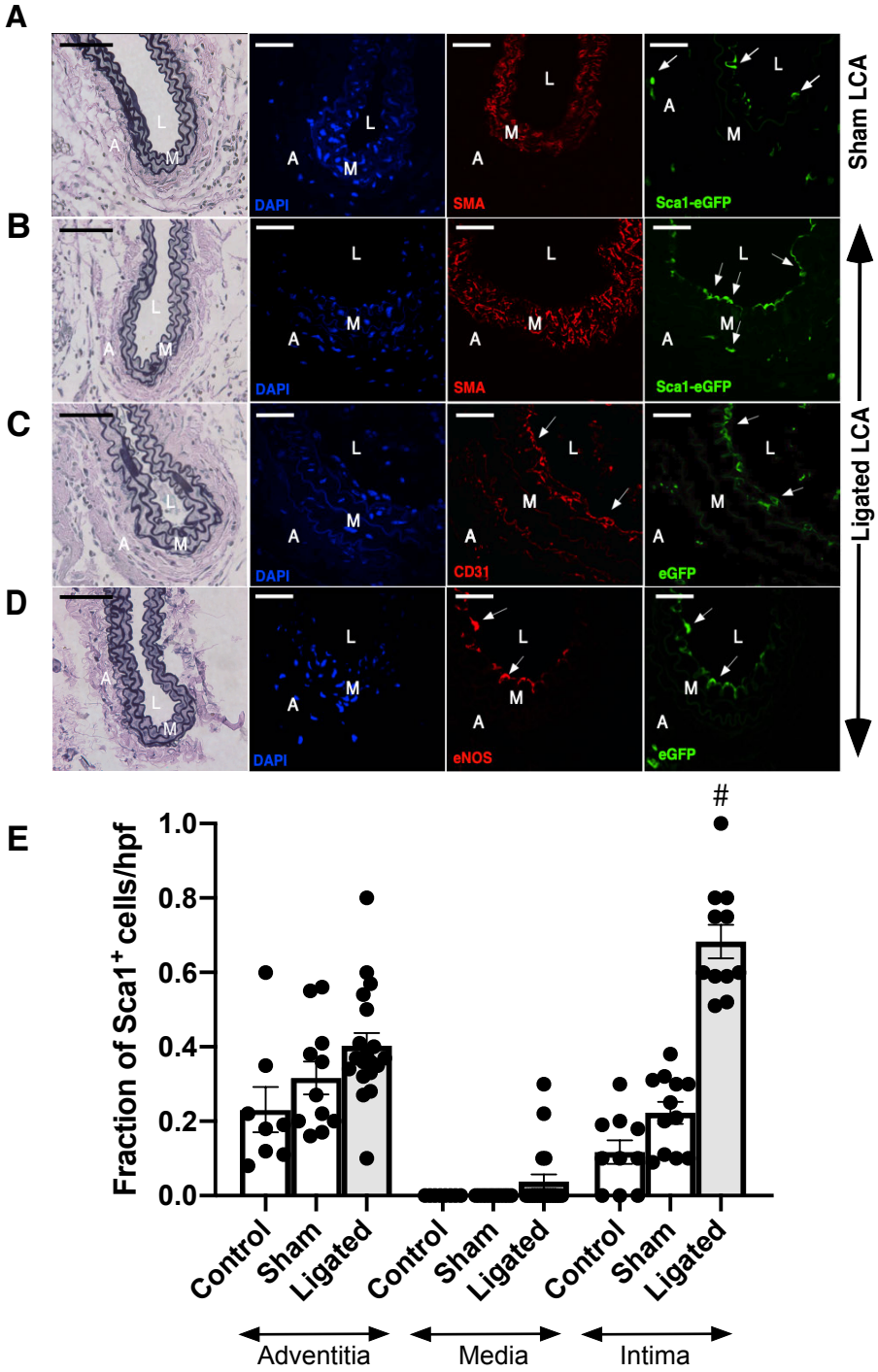
A
B
C
D
E
DAPI
SMA
Sca1-eGFP
CD31
eGFP
eNOS
Sham LCA
Ligated LCA
L
M
A
Fraction of Sca1+ cells/hpf
1.0
0.8
0.6
0.4
0.2
0.0
#
Control
Sham
Ligated
Adventitia
Media
Intima

Figure 2

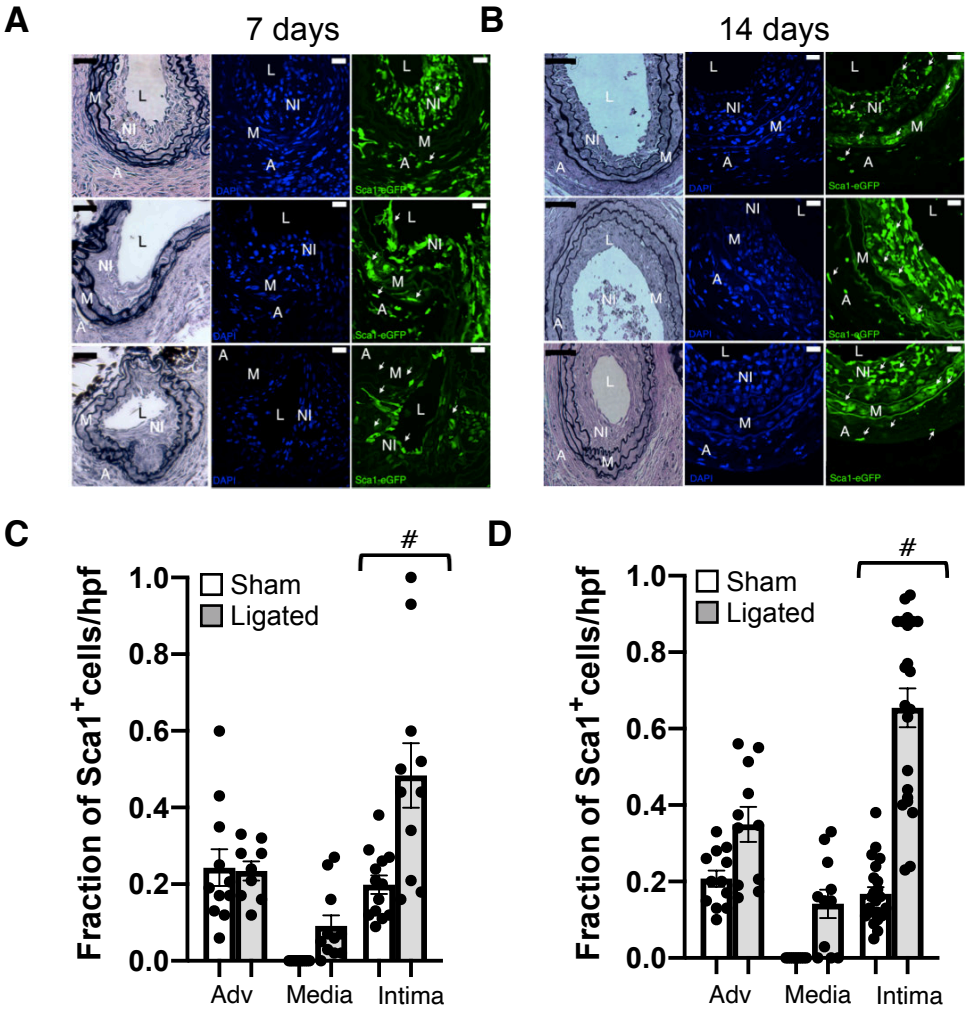
A
7 days
B
14 days
C
D
Sham
Ligated
Fraction of Sca1+cells/hpf
1.0
0.8
0.6
0.4
0.2
0.0
Adv
Media
Intima
#

Figure 3

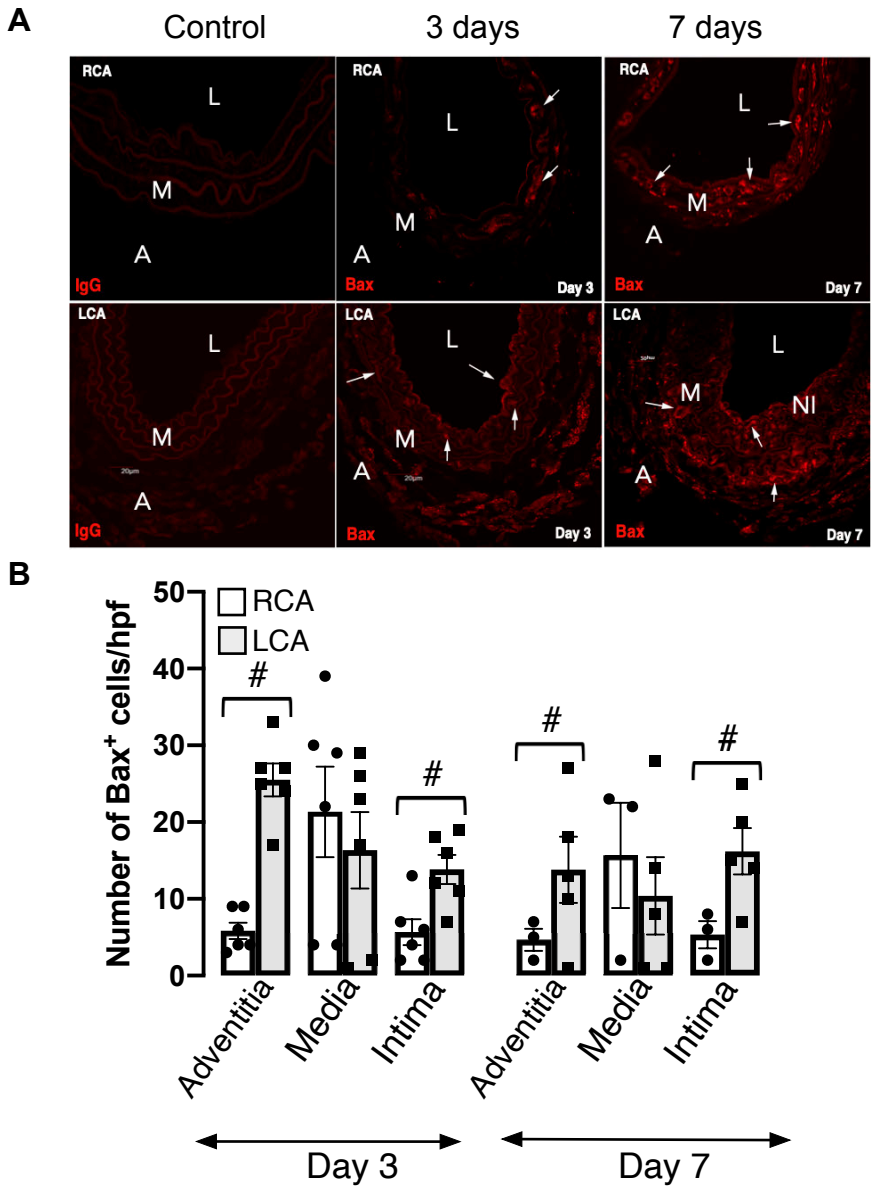
A
Control
3 days
7 days
RCA
L
M
A
IgG
Bax
Day 3
Day 7
LCA
NI
B
Number of Bax+ cells/hpf
50
40
30
20
10
0
RCA
LCA
#
Adventitia
Media
Intima
Day 3
Day 7

Figure 4

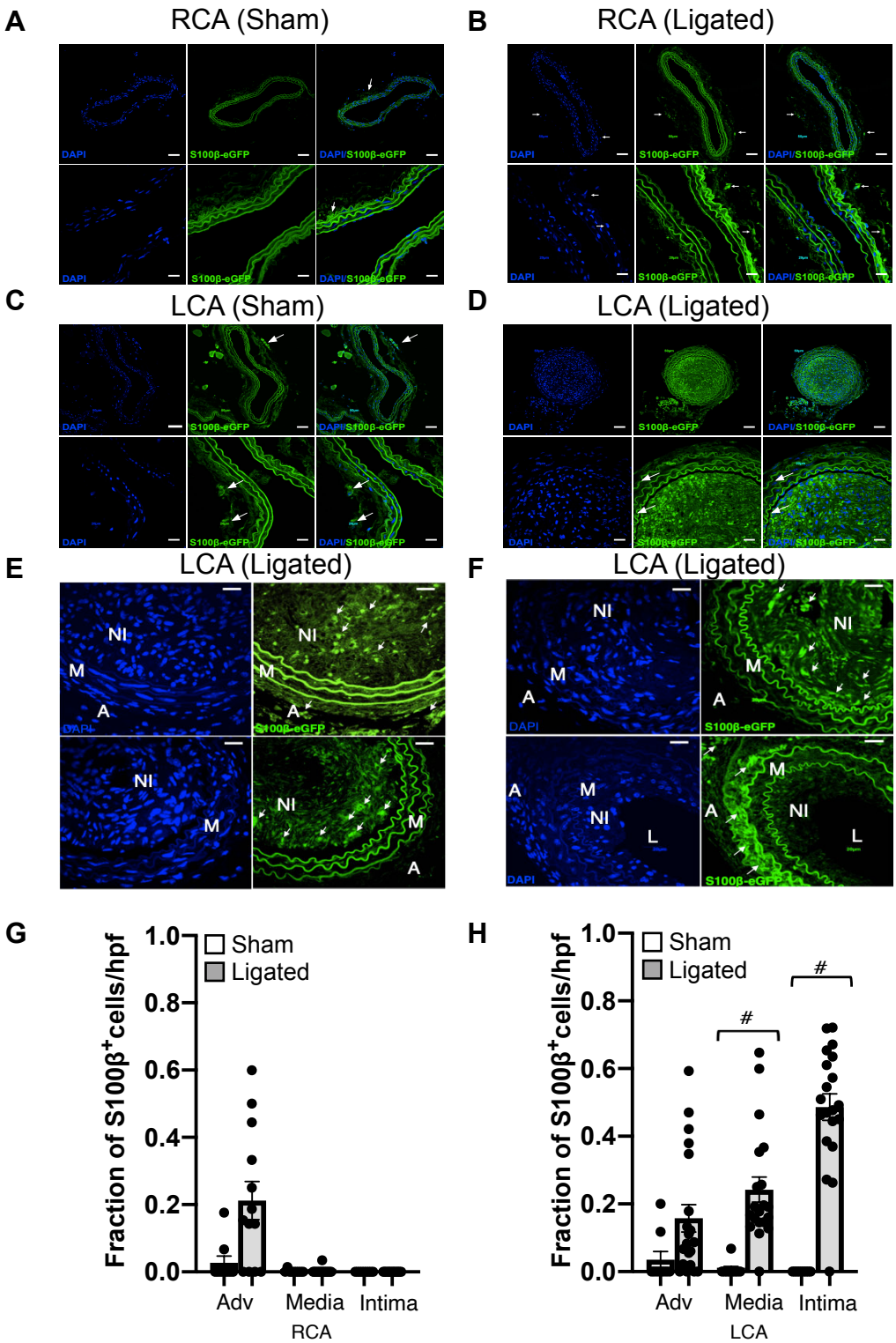
A
RCA (Sham)
B
RCA (Ligated)
C
LCA (Sham)
D
LCA (Ligated)
E
LCA (Ligated)
F
LCA (Ligated)
DAPI
S100β-eGFP
DAPI/S100β-eGFP
NI
M
A
L
G
H
Fraction of S100β+cells/hpf
1.0
0.8
0.6
0.4
0.2
0.0
Sham
Ligated
#
Adv
Media
Intima
RCA
LCA

Figure 5

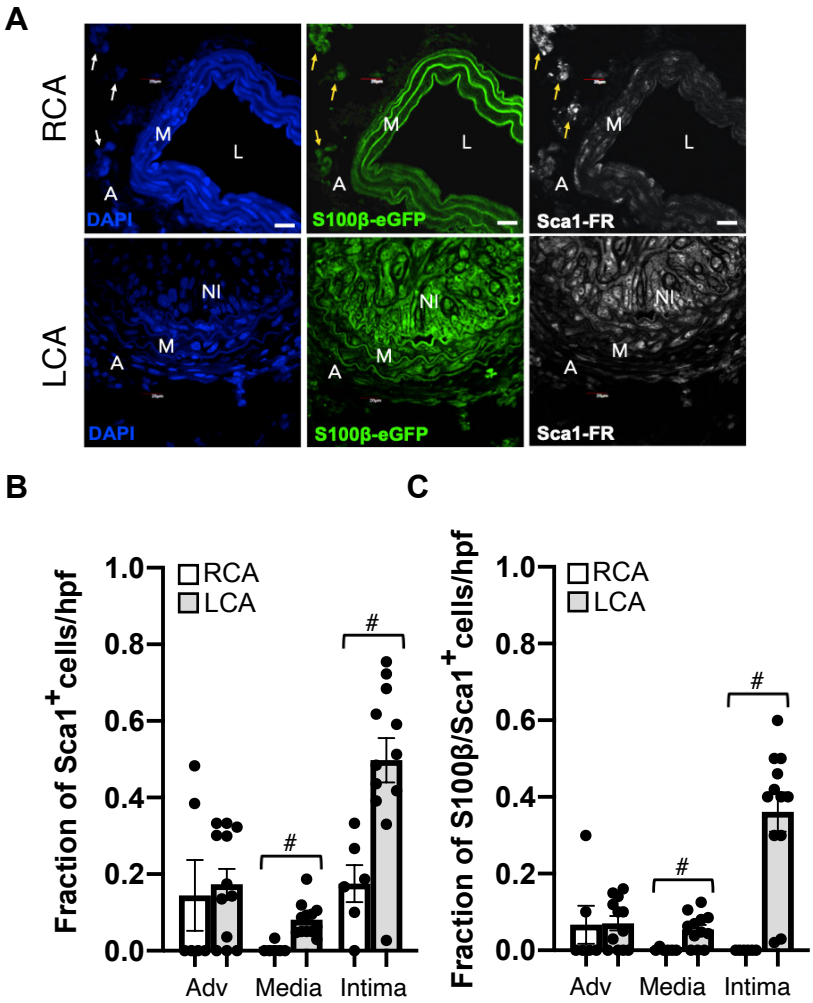
A
RCA
LCA
M
L
A
NI
DAPI
S100β-eGFP
Sca1-FR
B
C
RCA
LCA
Fraction of Sca1+cells/hpf
Fraction of S100β/Sca1+cells/hpf
1.0
0.8
0.6
0.4
0.2
0.0
#
Adv
Media
Intima

Figure 6

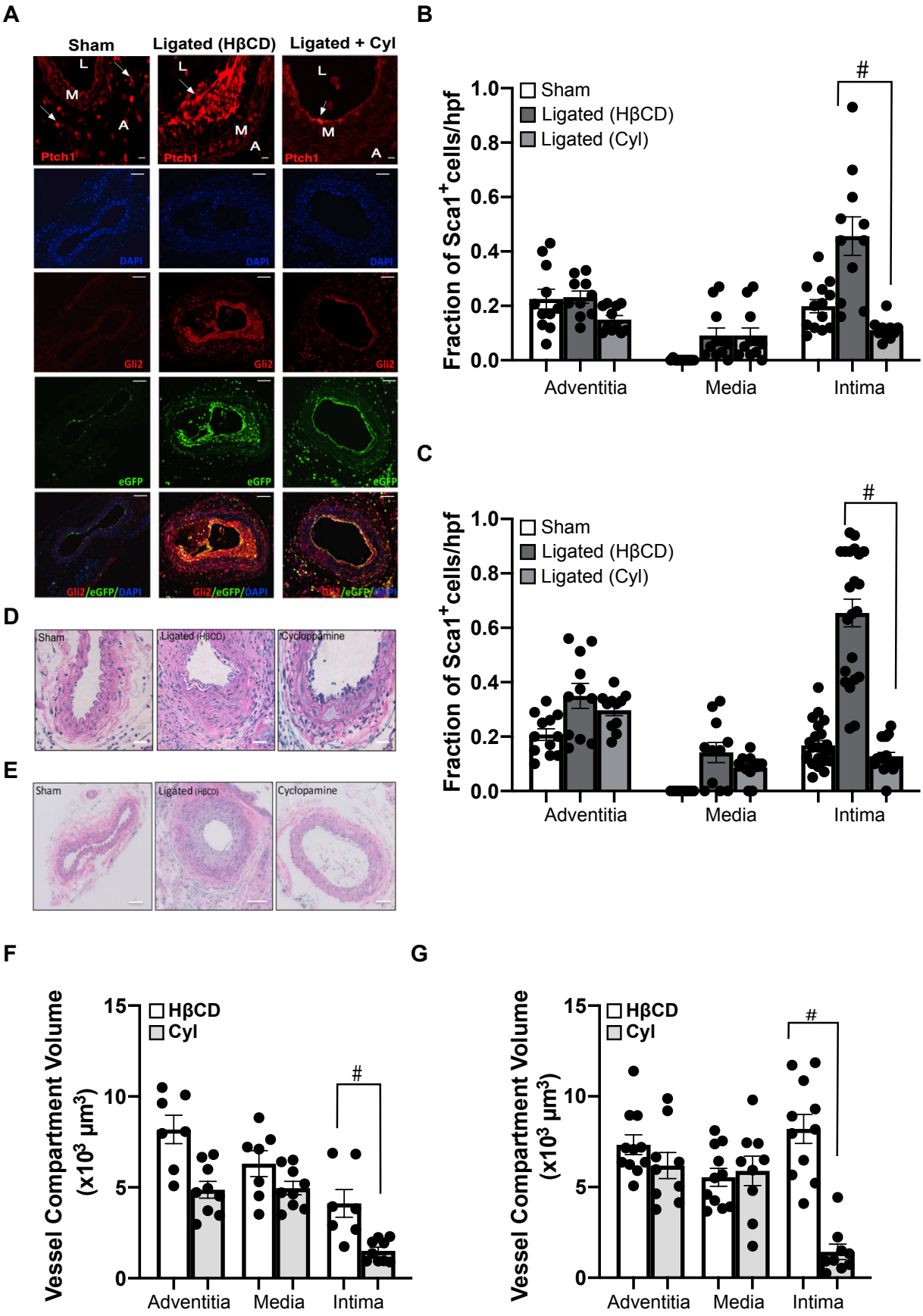
A
Sham
Ligated (HβCD)
Ligated + Cyl
L
M
A
Ptch1
DAPI
Gli2
eGFP
Gli2/eGFP/DAPI
B
Fraction of Sca1+cells/hpf
Sham
Ligated (HβCD)
Ligated (Cyl)
#
Adventitia
Media
Intima
C
Fraction of Sca1+cells/hpf
Sham
Ligated (HβCD)
Ligated (Cyl)
#
Adventitia
Media
Intima
D
Sham
Ligated (HβCD)
Cyclopamine
E
Sham
Ligated (HβCD)
Cyclopamine
F
Vessel Compartment Volume (x10³ µm³)
HβCD
Cyl
#
Adventitia
Media
Intima
G
Vessel Compartment Volume (x10³ µm³)
HβCD
Cyl
#
Adventitia
Media
Intima

Figure 7

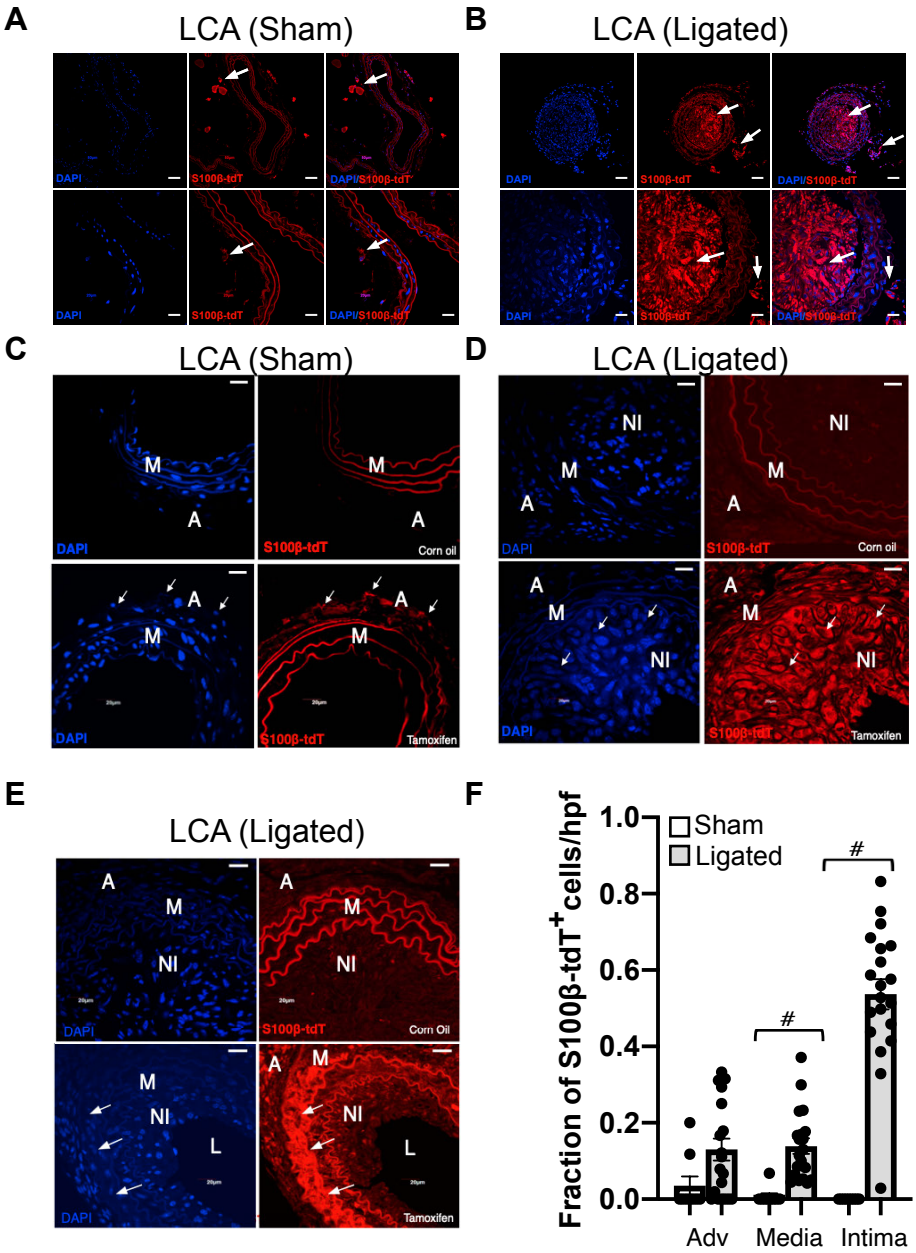
A
LCA (Sham)
B
LCA (Ligated)
C
LCA (Sham)
D
LCA (Ligated)
E
LCA (Ligated)
F
Fraction of S100β-tdT+ cells/hpf
Sham
Ligated
Adv
Media
Intima
DAPI
S100β-tdT
DAPI/S100β-tdT
Corn oil
Tamoxifen
M
A
NI
L

Figure 8

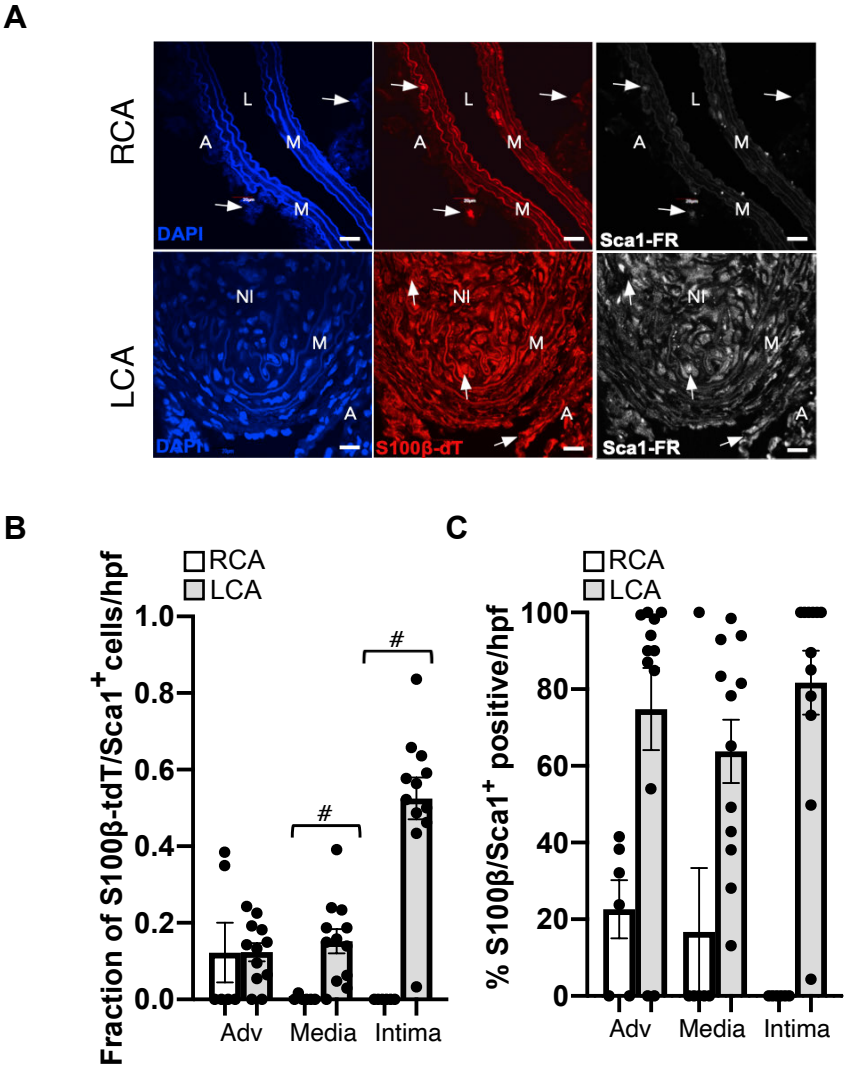
A
RCA
LCA
L
A
M
NI
DAPI
S100β-dT
Sca1-FR
B
RCA
LCA
Fraction of S100β-tdT/Sca1+cells/hpf
1.0
0.8
0.6
0.4
0.2
0.0
#
Adv
Media
Intima
C
RCA
LCA
% S100β/Sca1+ positive/hpf
100
80
60
40
20
0
Adv
Media
Intima

Figure 9

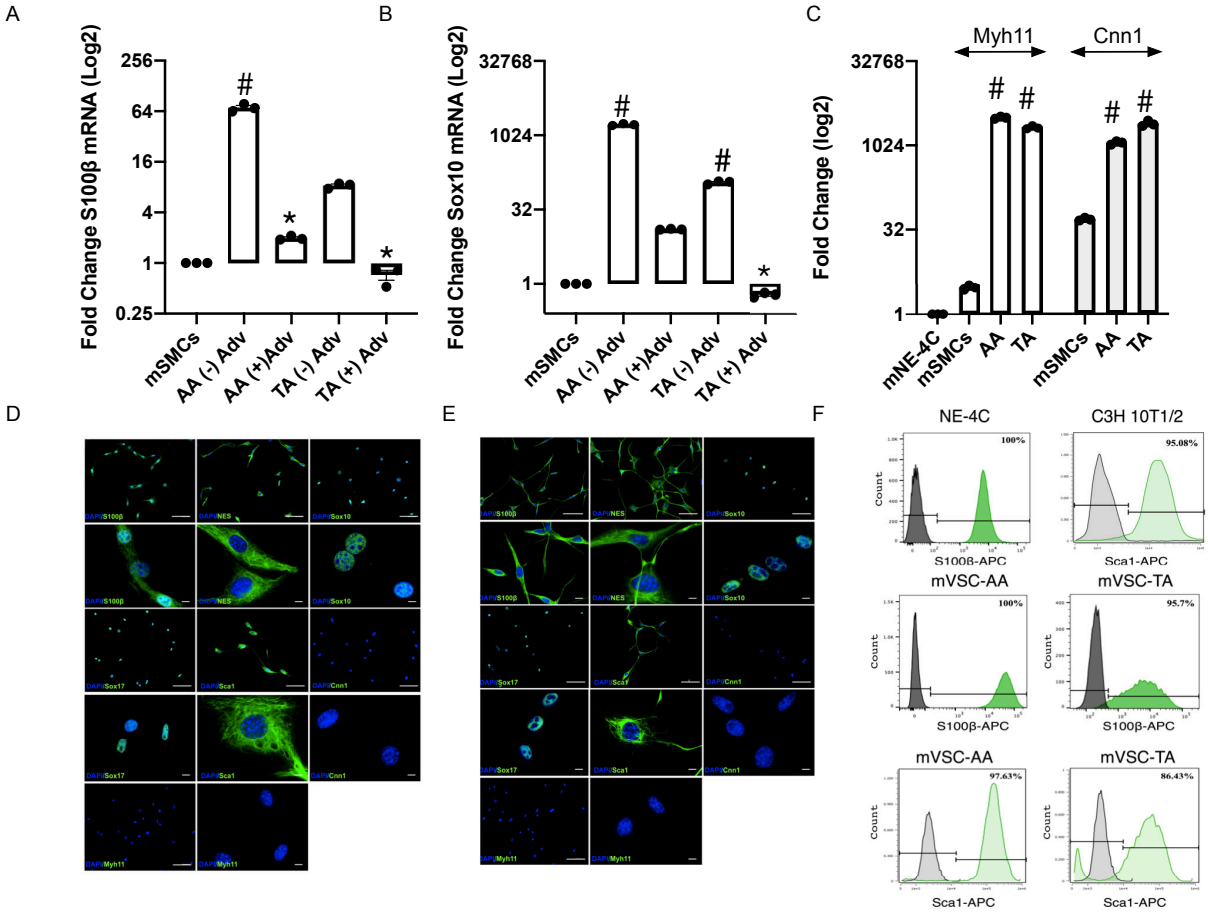
A
Fold Change S100β mRNA (Log2)
256
64
16
4
1
0.25
#
*
*
mSMCs
AA (-) Adv
AA (+)Adv
TA (-) Adv
TA (+) Adv
B
Fold Change Sox10 mRNA (Log2)
32768
1024
32
1
#
#
*
mSMCs
AA (-) Adv
AA (+)Adv
TA (-) Adv
TA (+) Adv
C
Fold Change (log2)
Myh11
Cnn1
32768
1024
32
1
#
#
#
#
mNE-4C
mSMCs
AA
TA
mSMCs
AA
TA
D
E
F
NE-4C
C3H 10T1/2
mVSC-AA
mVSC-TA
mVSC-AA
mVSC-TA
100%
95.08%
100%
95.7%
97.63%
86.43%
Count
S100β-APC
Sca1-APC

Figure 9 (contd)

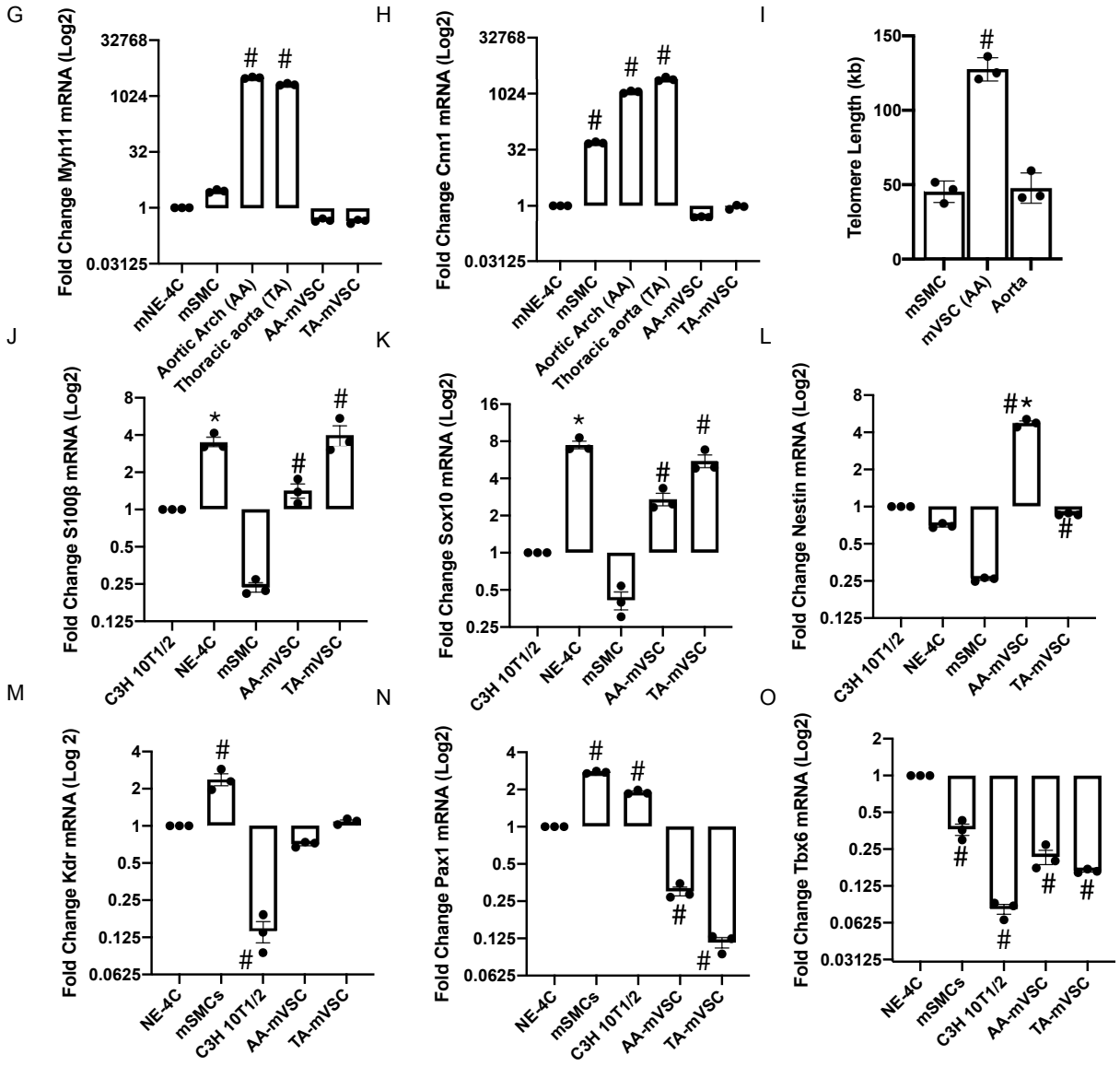

Figure 10

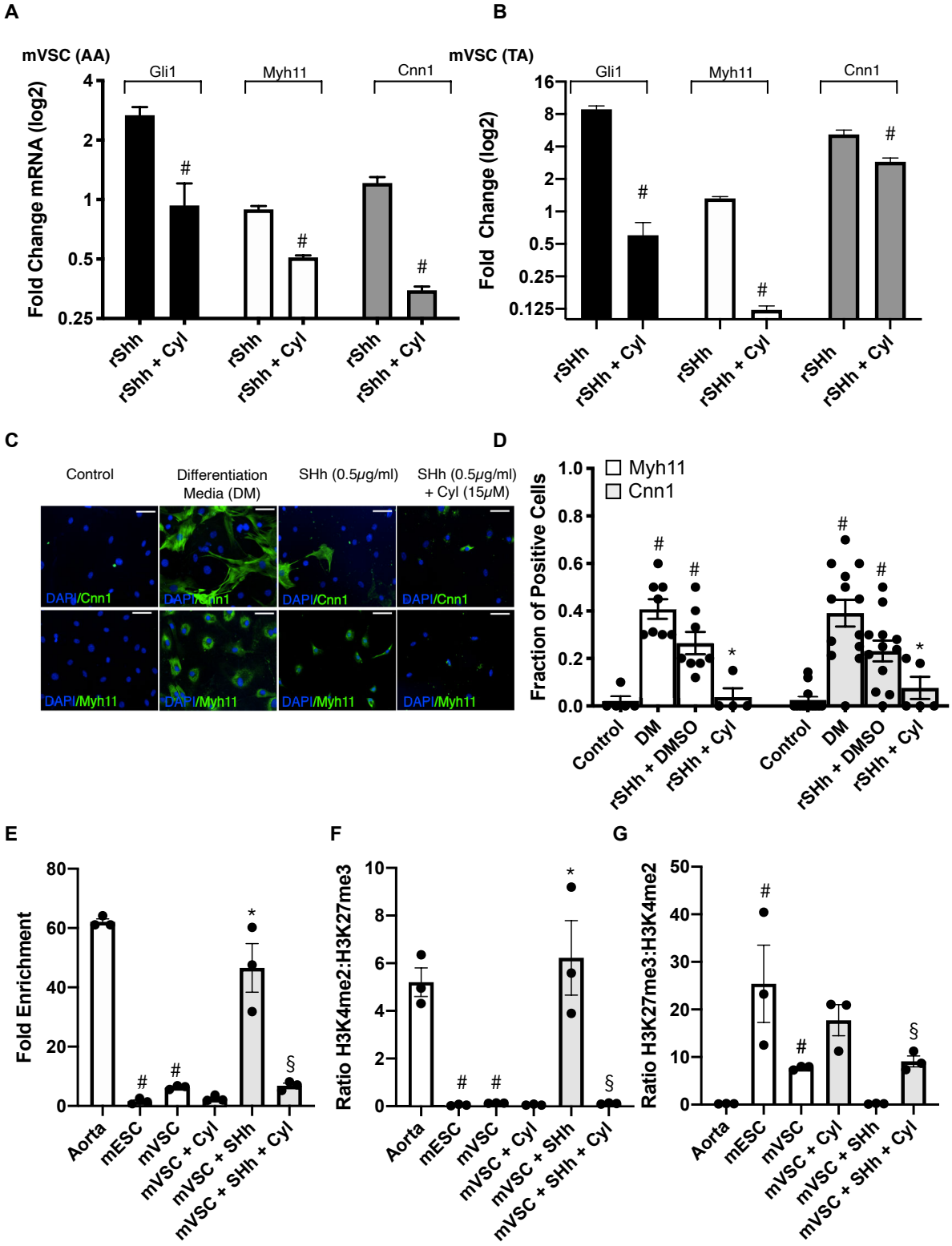
A
mVSC (AA)
Fold Change mRNA (log2)
Gli1
Myh11
Cnn1
rShh
rShh + Cyl
B
mVSC (TA)
Fold Change (log2)
rSHh
rSHh + Cyl
C
Control
Differentiation Media (DM)
SHh (0.5μg/ml)
SHh (0.5μg/ml) + Cyl (15μM)
DAPI/Cnn1
DAPI/Myh11
D
Fraction of Positive Cells
Myh11
Cnn1
Control
DM
rSHh + DMSO
rSHh + Cyl
E
Fold Enrichment
Aorta
mESC
mVSC
mVSC + Cyl
mVSC + SHh
mVSC + SHh + Cyl
F
Ratio H3K4me2:H3K27me3
G
Ratio H3K27me3:H3K4me2

Figure 11

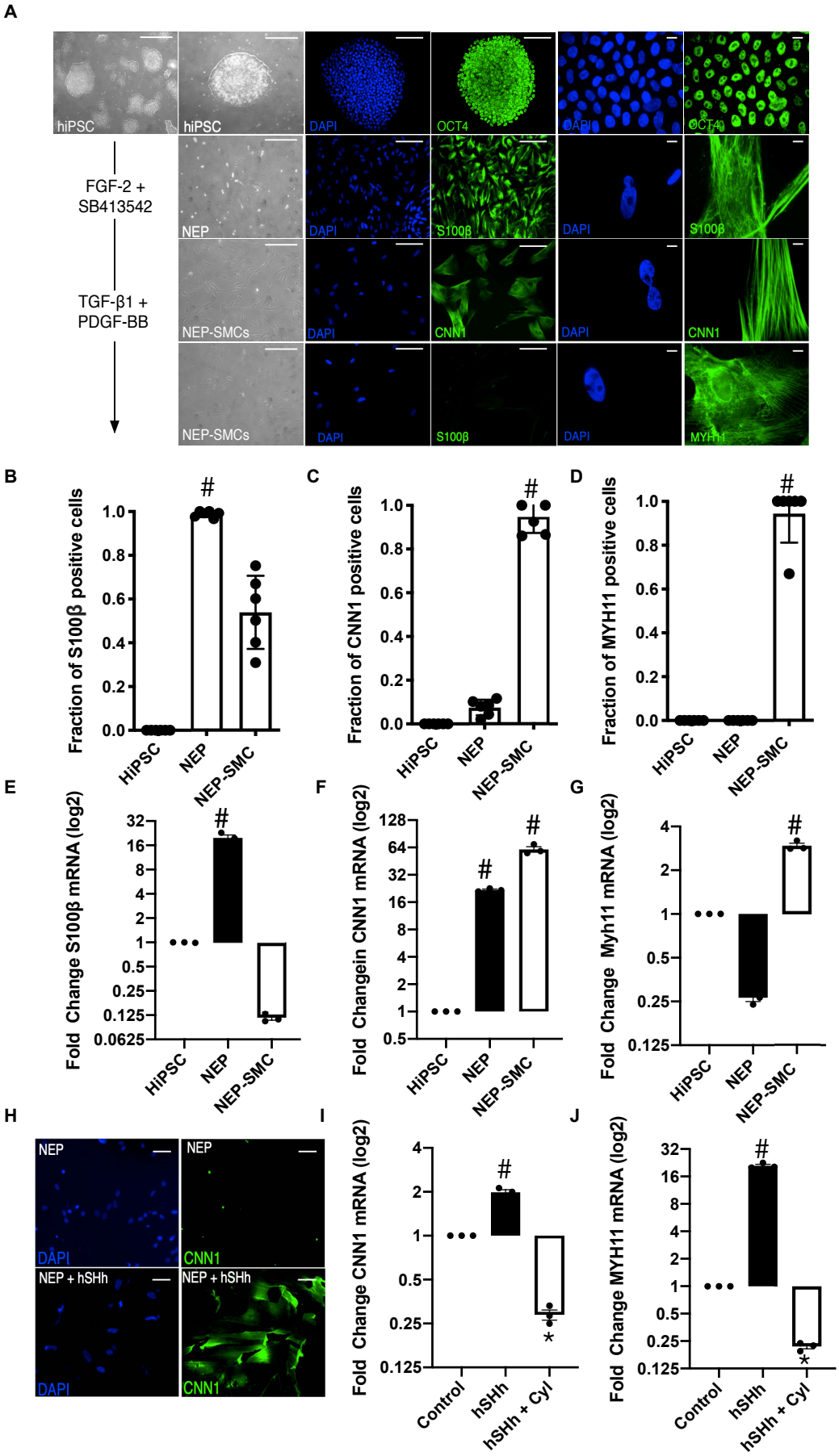
A
hiPSC
hiPSC
DAPI
OCT4
DAPI
OCT4
FGF-2 +
SB413542
NEP
DAPI
S100β
DAPI
S100β
TGF-β1 +
PDGF-BB
NEP-SMCs
DAPI
CNN1
DAPI
CNN1
NEP-SMCs
DAPI
S100β
DAPI
MYH11
B
Fraction of S100β positive cells
C
Fraction of CNN1 positive cells
D
Fraction of MYH11 positive cells
HiPSC
NEP
NEP-SMC
E
Fold Change S100β mRNA (log2)
F
Fold Changein CNN1 mRNA (log2)
G
Fold Change Myh11 mRNA (log2)
H
NEP
DAPI
CNN1
NEP + hSHh
I
Fold Change CNN1 mRNA (log2)
J
Fold Change MYH11 mRNA (log2)
Control
hSHh
hSHh + Cyl

Figure 12

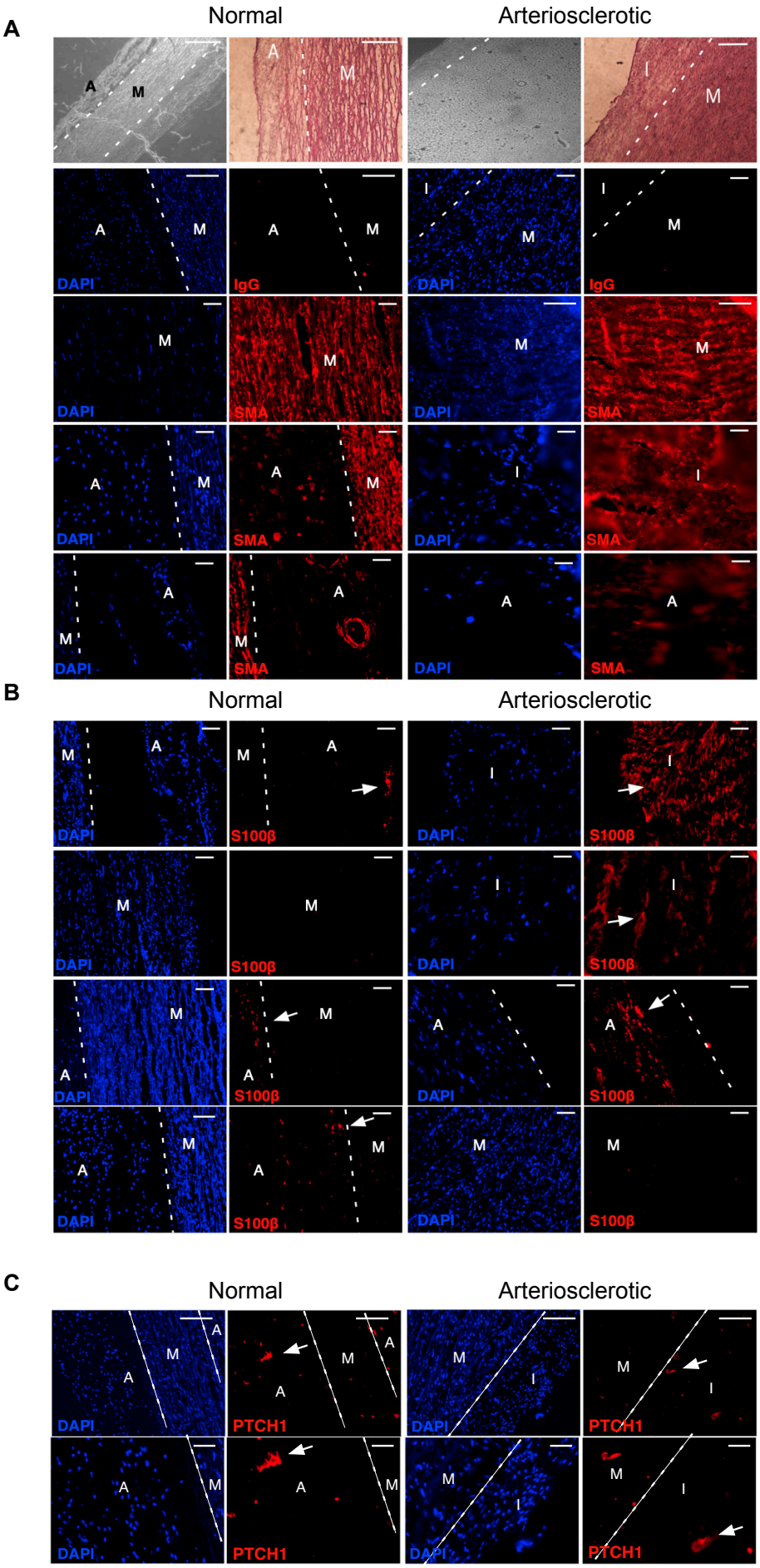

Supplemental Figures

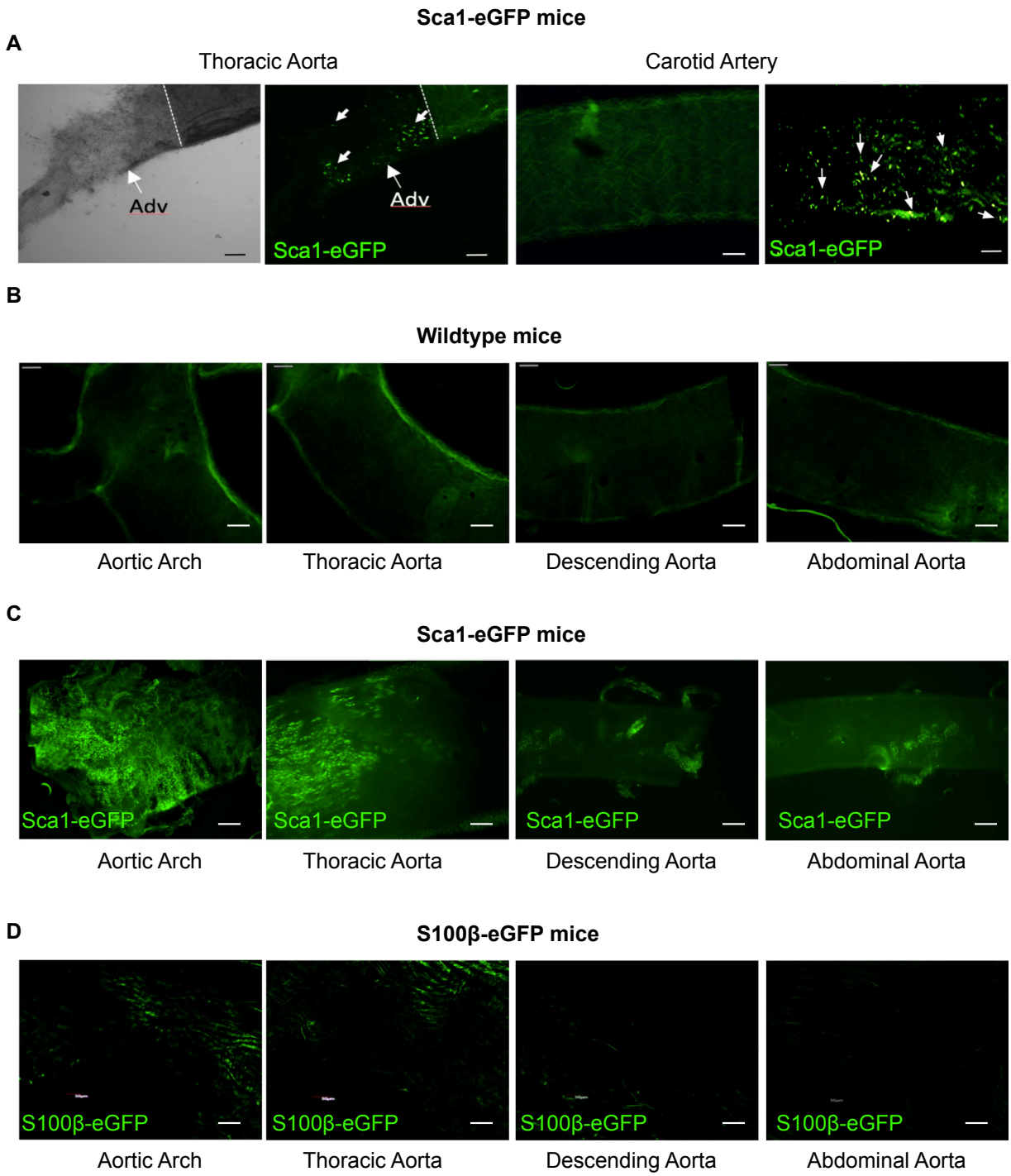

Figure S1 (related to Figure 1 and 2). **Sca1$^+$ and S100β$^+$ cells are present in perivascular regions of murine arteries.** (A) Whole mount analysis of Sca1-eGFP expression in mouse aorta and carotid artery of Sca1-eGFP transgenic mice, (B) wildtype control mice and (C) Sca1-eGFP expression aortic arch, thoracic aorta, descending aorta and abdominal aorta. (D) S100β-eGFP expression in aortic arch, thoracic aorta, descending aorta and abdominal aorta. Each image is representative of 5 images from 3 animals.

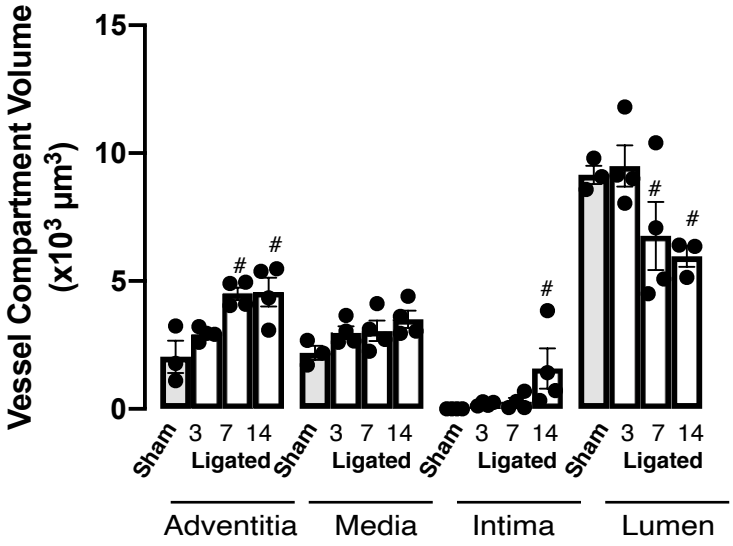

Figure S2 (related to Figure 1 and 2). **Iatrogenic flow restriction following partial ligation of the left carotid artery (LCA) of Sca1-eGFP transgenic mice results in intimal thickening and vessel remodelling.** Morphometric analysis of adventitial, medial, intimal and luminal volumes following partial ligation of the left carotid artery compared to sham controls. Data are the mean ± SEM of 4 animals, #p≤ 0.05 vs sham.

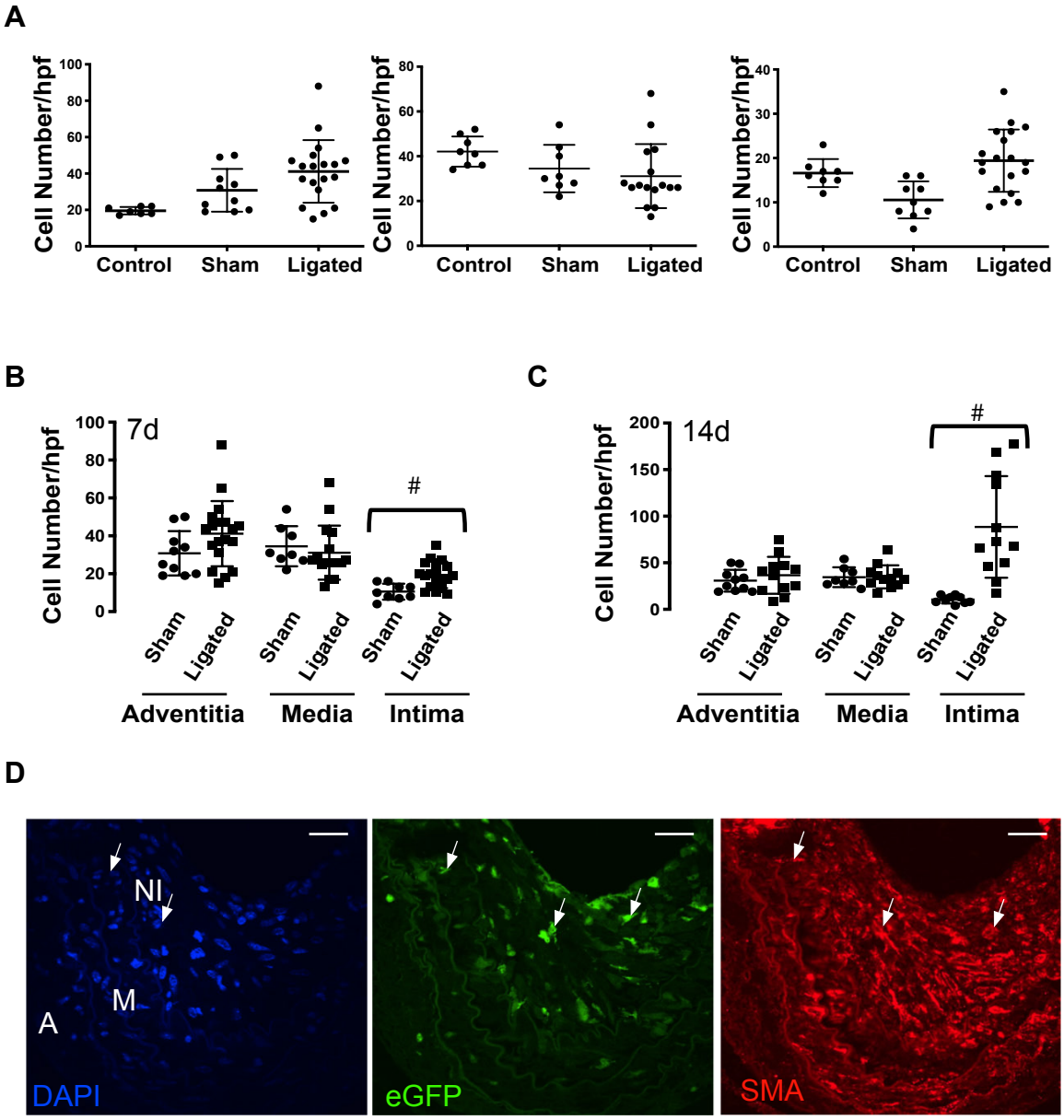

Figure S3 (related to Figure 1 and 2). **Iatrogenic flow restriction following partial ligation of the left carotid artery (LCA) of Sca1-eGFP transgenic mice results in increased cell number and co-localisation of Sca1/SMA cells.** The number of DAPI nuclei/hpf in cross-sections of adventitia, media and intima following partial ligation of the left carotid artery (LCA) after (A) 3d (B) 7d and (C) 14d compared to untouched (control) and sham. Data are the mean ± SEM of 3-5 representative images per animals, n=3, #p≤ 0.05. (D) Immunohistochemical staining showing co-localisation of Sca1$^+$ cells and SMA$^+$ cells within medial and intimal layers of Sca1-eGFP transgenic mice following partial ligation of the left carotid artery (LCA) after 14 days. Data are representative of 5 images per animal.

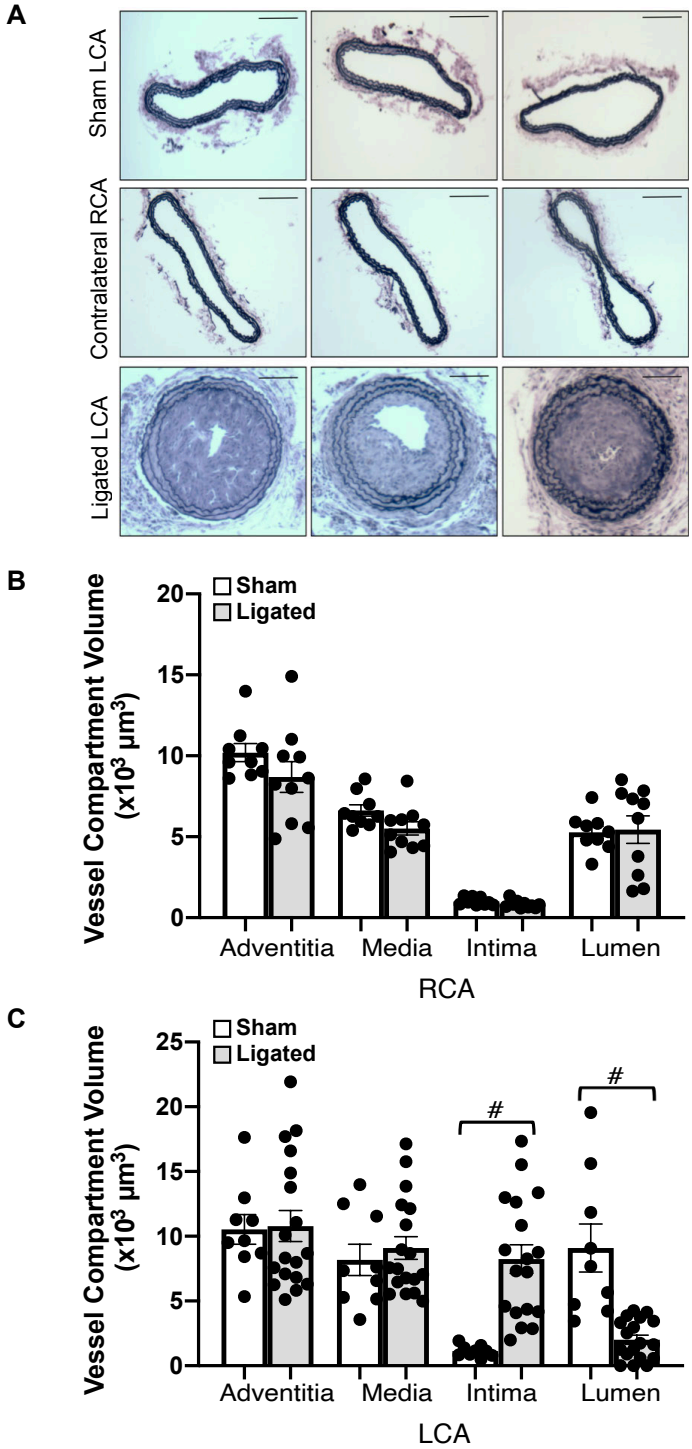

Figure S4 (related to Figure 4 and 5). **Iatrogenic flow restriction following complete ligation of the left carotid artery (LCA) of S100β-eGFP transgenic mice results in intimal thickening and vessel remodelling.** (A) Verhoeff-Van Gieson stained sections and (B, C) morphometric analysis of adventitial, medial, intimal and luminal volumes following complete ligation of the left carotid artery (LCA) for 21 d compared to the contralateral right carotid artery (RCA) controls. Data are the mean ± SEM of 10 animals, #p≤ 0.05 vs sham controls.

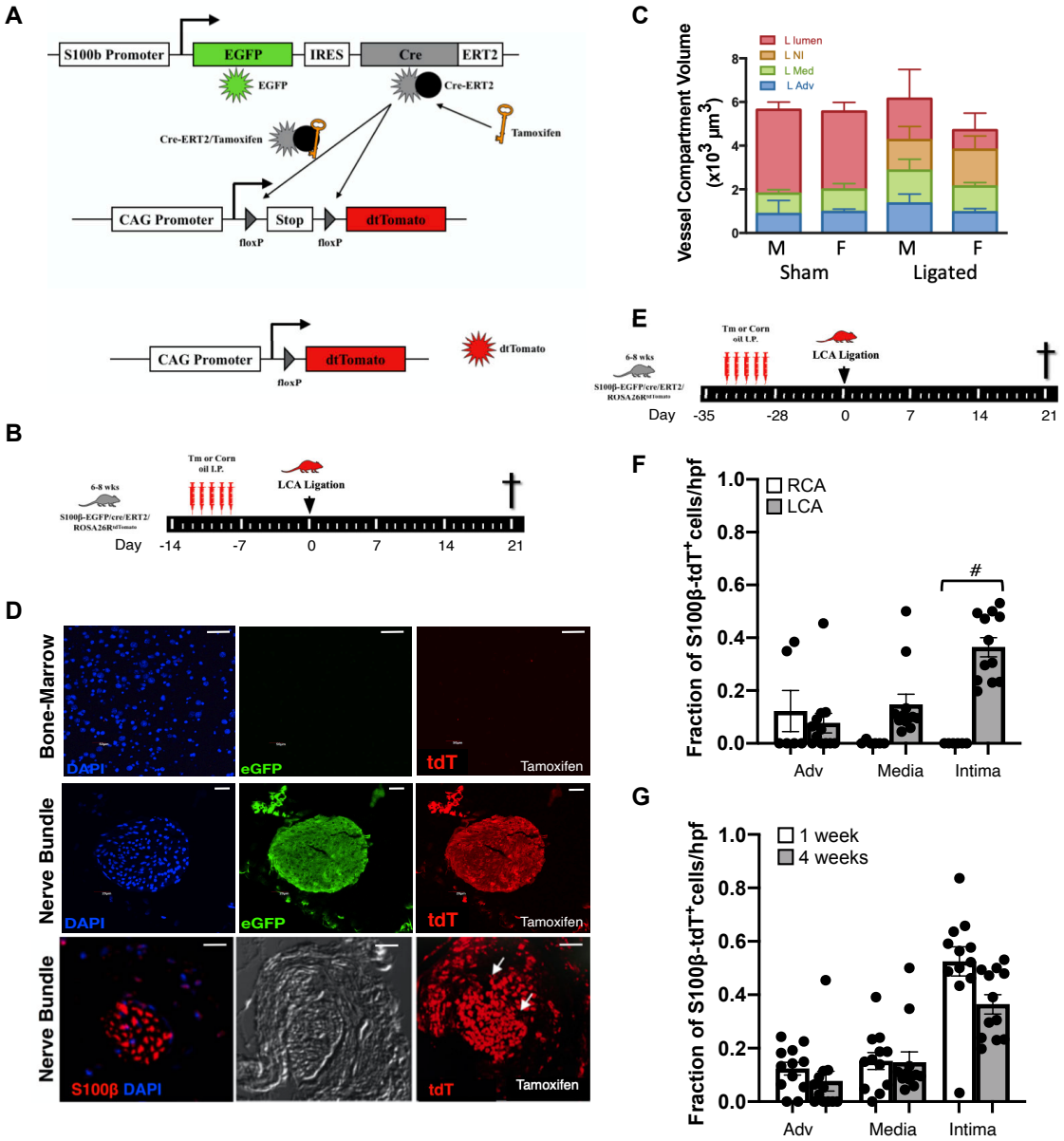

Figure S5 (related to Figure 7 and 8). **S100β⁺ cell contribution following iatrogenic flow restriction of the left carotid artery (LCA) of S100β- CreERT2-Rosa26-tdTomato transgenic mice.** (A) schematic diagram showing genetic lineage tracing by S100β-CreERT2-Rosa26-tdTomato. (B) Schematic diagram showing protocol for Tm injections before ligation after 1 week Tm washout. (C) Morphometric analysis of adventitial, medial, intimal and luminal volumes in male and female S100β-CreERT2-Rosa26-tdTomato mice following complete ligation of the left carotid artery (LCA) for 21 days. (D) S100β-tdT expression in bone marrow smears and the carotid sinus nerve and validated using anti-eGFP and anti-tdT antibodies. (E) Schematic diagram showing protocol for Tm injections before ligation after 4 week Tm washout protocol. (F) The fraction of S100β-tdT⁺ cells within the adventitial, medial, intimal layers of LCA 1 after 4 week washout, p≤ 0.05 vs RCA. (G) Comparison of the fraction of S100β-tdT⁺ cells within the adventitial, medial, intimal layers of LCA between 1 week and 4 week Tm washout protocols. Data are the mean ± SEM of 3-5 representative images from 3 animals, #p≤ 0.05 vs RCA controls.

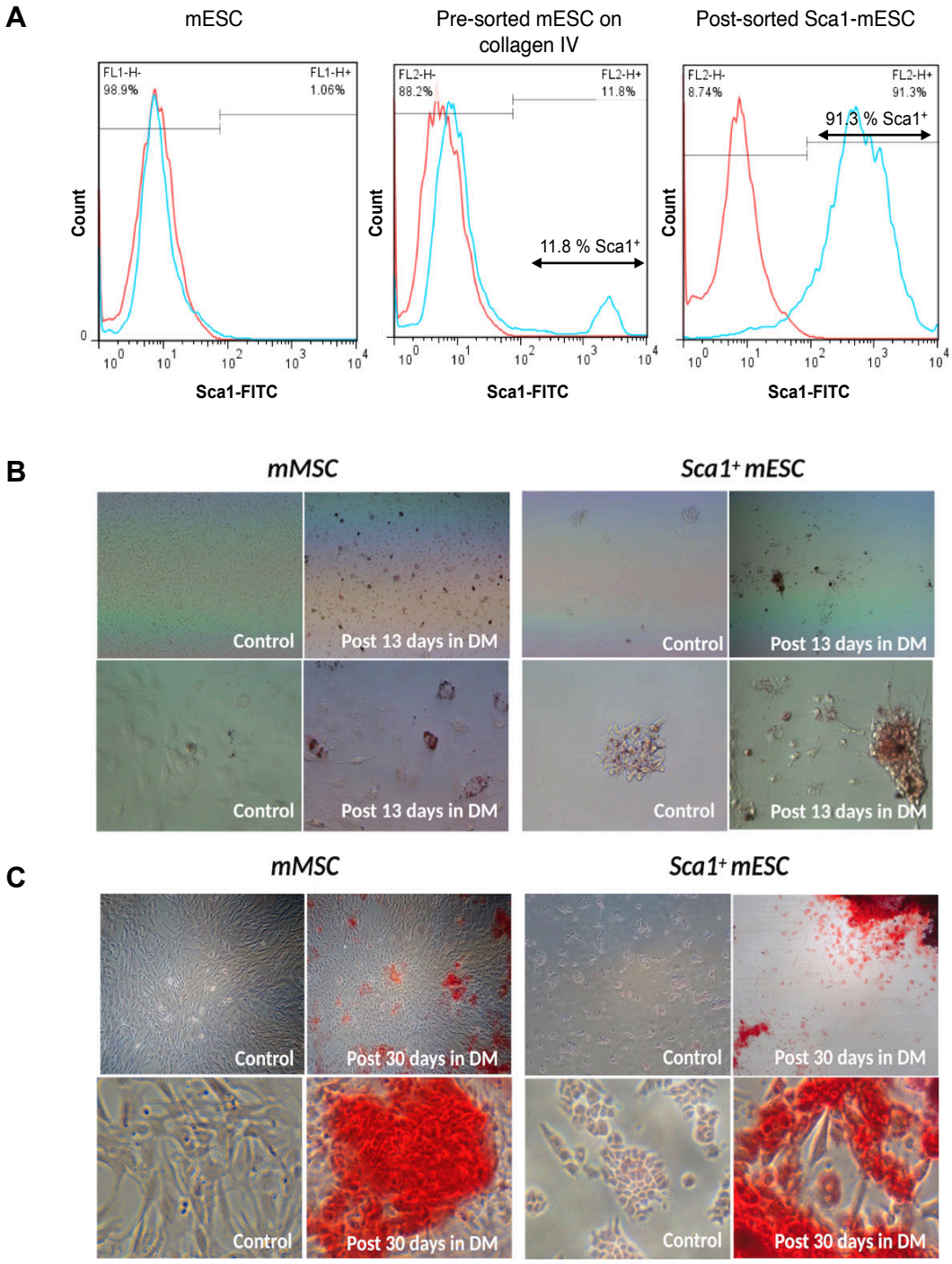

Figure S6 (related to Figure 9). **Multipotency of mESC derived Sca1/S100β⁺ cells *in vitro* in response to adipogenic and osteogenic inductive media.** (A) Flow cytometry of murine ESC-derived Sca1⁺ cells generated from mESCs grown on collagen IV and purified. (B) Oli Red O staining following adipogenic differentiation of Sca1-mESCs and MSCs and (C) Alizarin Red staining following osteogenic differentiation of Sca1-mESCs and MSCs. Data are representative of 3 individual experiments.

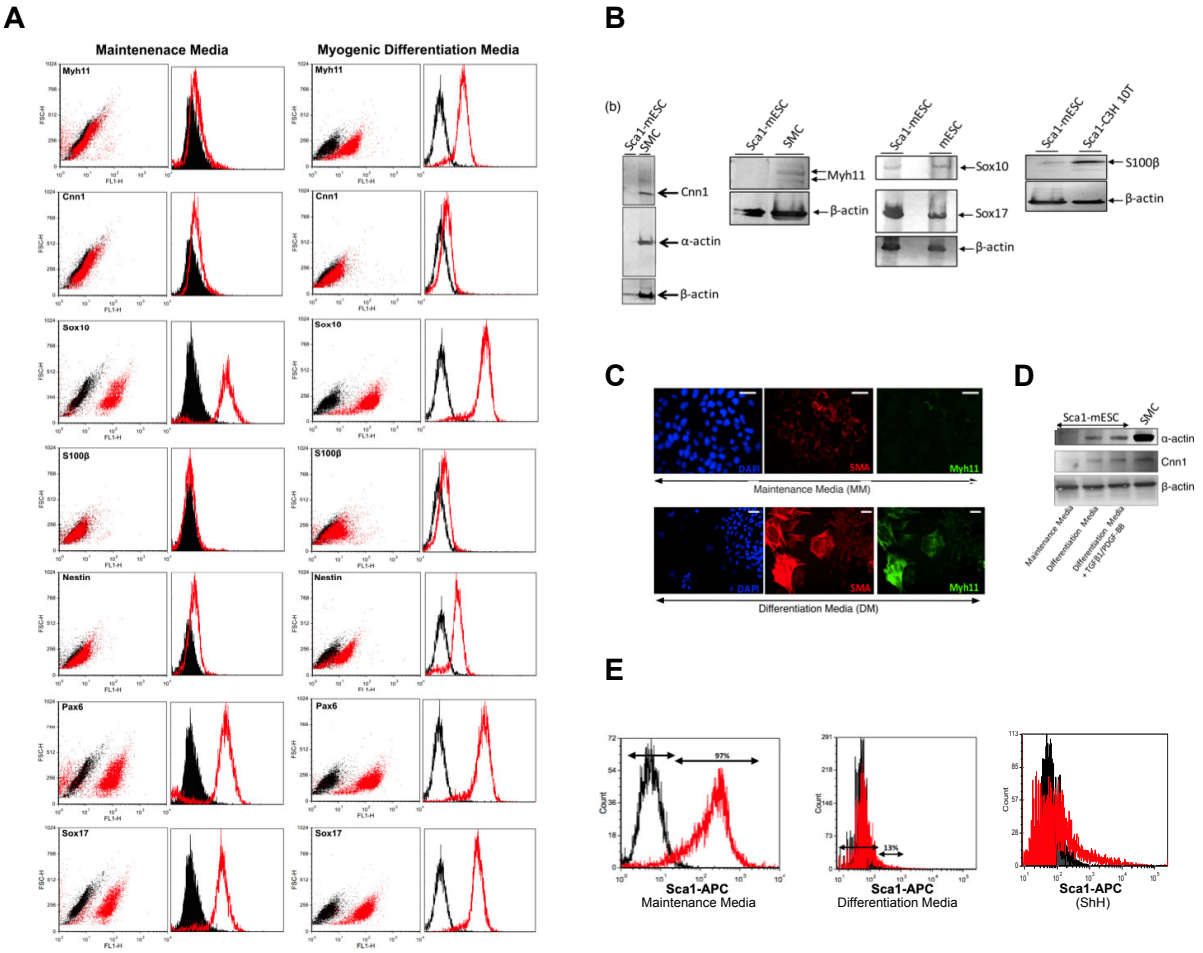

Figure S7 (related to Figure 10). **Multipotent mESC derived Sca1/S100β^{+} cells undergo myogenic SMC differentiation *in vitro*.** (A) Flow cytometry analysis of SMC differentiation markers (Myh11 and Cnn1) and NE stem cell markers (Sox10, Sox17, S100β, Pax6 and Nestin) in mESC-Sca1^{+} cells grown in maintenance media and myogenic differentiation media. (B) Immunoblot analysis of mESC derived Sca1/S100β cell markers. (C) Immunocytochemical analysis and (D) immunoblot analysis of SMC differentiation markers (Myh11 and Cnn1) following myogenic differentiation. Scale bar= 50µm. (E) Flow cytometry analysis of Sca1 expression following myogenic differentiation and SHh treatment (0.5µg/ml). Data are representative of three independent experiments per group.

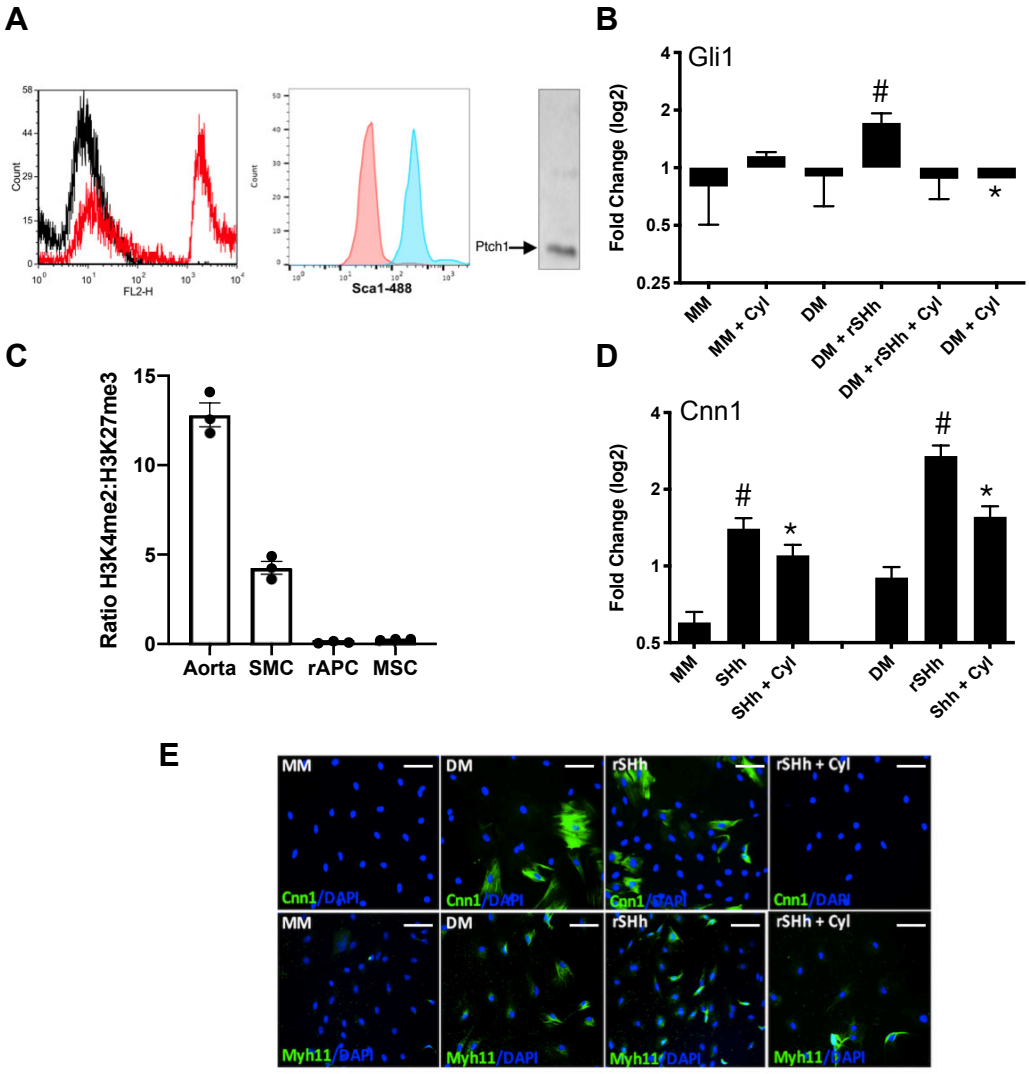

Figure S8 (related for Figure 10 and 11). **Rat adventitial Sca1/S100β⁺ cells undergo myogenic SMC differentiation *in vitro* in response to hedgehog**. (A) Flow cytometry analysis of Sca1 expression in purified adventitial progenitor stem cells (APC). (B) Fold change in rSHh stimulation of Gli1 expression in the absence or presence of cyclopamine. MM; maintenance media, DM: Differentiation media, #p≤ 0.05, *p≤ 0.05 vs rSHh, n=3. (C) ChIP analysis of H3K4me2 enrichment at the Myh11 promoter in fresh rat aortic tissue, rat SMCs, Sca1⁺ rAPC and rat MSCs. (D) Fold change in Cnn1 expression in the absence or presence of cyclopamine, #p≤ 0.05, *p≤ 0.05 vs rSHh, n=3. (E) immunocytochemical analysis of SMC differentiation markers (Myh11 and Cnn1) following myogenic differentiation of Sca1⁺ rAPCs. Data are representative of three independent experiments per group.

Supplementary Table I

Antibodies and their corresponding dilutions used in immunohistochemistry.

Antibody/Product Name	Supplier/Product Number	Dilutions
Rat anti-mouse Sca1/Ly6A/E antibody [D7] (FITC) antibody	Abcam (ab25031)	1/200
Rabbit anti-mouse/rat alpha smooth muscle cell α-actin antibody	Abcam (ab5694)	1/200
Anti-Patched / PTCH1 antibody, Mouse monoclonal	Abcam (Ab55629)	1/100
Anti-Actin, α-Smooth Muscle antibody, Mouse monoclonal	Sigma (A5228)	1/200
Anti-S100-β (CT) Antibody, clone EP1576Y, rabbit monoclonal	Millipore (04-1054)	1/100
Chicken anti-GFP antibody	Abcam (ab13970)	1/1000
Rabbit Anti-RFP/dT antibody	Abcam (ab62341)	1/1000

Supplementary Table II

Antibodies and their corresponding dilutions used in immunocytochemistry/western blot.

Antibody/Product Name	Supplier/Product Number	Dilutions
Mouse anti-mouse/rat nestin [Rat-401]	Abcam (ab11306)	1/200
Rabbit anti-mouse Calponin [EP798Y]	Abcam (ab46794)	1/200
Goat anti-mouse/rat/human smooth muscle Myosin heavy chain	Santa Cruz (sc-79079)	1/200

Mouse anti-human/rat SOX10	R&D System (MAB2864)	1/100
Mouse anti-human SOX17	R&D System (MAB1924)	1/100
Rabbit Anti-S100β	Merck Millipore (ABN59)	1/100
Rabbit Anti-mouse/rat S100β [EP1576Y]	Abcam (ab52642)	1/100
Rabbit anti-mouse/rat Sca1	Millipore (AB4336)	1/100
Alexa Fluor® 488 Goat anti-mouse IgG	Invitrogen (A-11001)	1/1000
Alexa Fluor® 488 Goat anti-rabbit IgG	Invitrogen (A-11008)	1/1000
Alexa Fluor® 488 Donkey anti-goat IgG	Invitrogen (A-11055)	1/1000

Supplementary Table III

Antibodies used in Chromatin Immunoprecipitation (ChIP)

Antibody/Product Name	Supplier/Product Number
Rabbit anti-mouse Tri-Methyl-Histone H3 (Lys27) [C36B11]	Cell Signalling Technology (9733S)
Rabbit anti-mouse Di-Methyl-Histone H3 (Lys4) [C64G9]	Cell Signalling Technology (9725S)
Normal Rabbit IgG (ChIP graded)	Cell Signalling Technology (2729)

Supplementary Table IV

Customised primers used in this study from Integrity DNA Technology (IDT).

Customised primer		Sequences
Mm_Sm-mhc (Myh11)	Forward	5' - GCA GTG AGC TCT CAG TCA TC - 3’
	Reverse	5' - CAA TGC CTC CTC TGA CAA GT - 3'

Mm_Cnn1	Forward	5’ - GCT TGT CTG CTG AAG TAA AGA AC - 3'
	Reverse	5’ - TCC ATG AAG TTG TTC CCG ATG - 3'
Mm_Gli1	Forward	5' - TTG GAT TGA ACA TGG CGT CT - 3'
	Reverse	5' - CCT TTC TTG AGG TTG GGA TGA - 3'
Mm_Hprt	Forward	5’ - GGC TAT AAG TTC TTT GCT GAC CTG C - 3'
	Reverse	5’ - GCT TGC AAC CTT AAC CAT TTT GGG - 3'
Mm_Gaphd	Forward	5’ - GCC TCC AAG GAG TAA GAA AC - 3'
	Reverse	5’ - GCC TCC AAG GAG TAA GAA AC - 3'
Mm_ Sm-mhc	Forward	5’ - CCC TCC CTT TGC TAA ACA CA - 3'
(Myh11) for ChIP PCR	Reverse	5’ - CCA GAT CCT GGG TCC TTA CA - 3'

Primers used in this study from QIAGEN.

Primer	Product Name	Product Code
mHprt-1	Mm_Hprt_1_SG QuantiTect Primer Assay	QT00166768
mS100β	Mm_S100β_1_SG QuantiTect Primer Assay	QT00151536
mSox10	Mm_Sox10_1_SG QuantiTect Primer Assay	QT00295204
mNestin	Mm_Nes_1_SG QuantiTect Primer Assay	QT00316799
mGapdh	Mm_Gapdh_3_SG QuantiTect Primer Assay	QT01658692
mPax6	Mm_Pax6_1_SG QuantiTect Primer Assay	QT01052786
mPax1	Mm_Pax1_1_SG QuantiTect Primer Assay	QT01052779
mKdr	Mm_Kdr_1_SG QuantiTect Primer Assay	QT00097020
mTbx6	Mm_Tbx6_1_SG QuantiTect Primer Assay	QT00098861
hCNN1	Hs_CNN1_1_SG_QuantiTech Primer	QT00067718
hHPRT1	Hs_HPRT1_1_SG QuantiTect Primer	QT00059066
hMYH11	Hs_MYH11_1_SG QuantiTech Primer	QT00069391
hS100β	Hs_S100B_1_SG QuantiTect Primer Assay	QT00059164

rCnn1	Rn_Cnn1_1_SG QuantiTect Primer	QT01081115
rGli1	Rn_Gli1_1_SG QuantiTect Primer	QT01290324
rGapdh	Rn_Gapd_1_SG QuantiTect Primer	QT00199633
rHprt-1	Rn_Hprt1_1_SG QuantiTect Primer	QT00199640

Supplementary Table V

Antibodies and their corresponding dilutions used in Flow Cytometry.

Antibody/Product Name	Supplier/Product Number	Dilutions
Rat anti-mouse Sca1 (Ly-6A/E) [E13-161.7]	STEMCELL Technology (60032)	1/100
Rat anti-mouse IgG2a, kappa Isotype [RTK2758]	STEMCELL Technology (60076)	1/100
Rabbit Anti-mouse/rat S100β [EP1576Y]	Abcam (ab52642)	1/100
Normal Rabbit IgG (F graded)	Cell Signalling Technology (2729)	1/100
Rabbit-IgG Alexa-Fluor 488, Isotype Ctl	Bioss (bs-0295p-A488)	1/100
FITC Rat IgG2a, κ Isotype Control	BioLegend (400505)	1/100
PE Rat IgG2a, κ Isotype Control	MSC (400507)	1/100
Anti-Mouse Sca1	Miltenyi Biotech (130-093-222)	1/100
Anti-Mouse Sca1 Antibody, Clone	STEMCELL (E13-161.7 60032)	1/100
Monoclonal anti-Nestin Clone 10C2 Mouse IgG	ThermoScientific (MA1-110)	1/100
Polyclonal Rabbit anti-Pax6	Abcam (Ab5790)	1/100
Monoclonal Rabbit anti-Sox10 Clone EPR4007 Rabbit IgG	Abcam (Ab155279)	1/100
Polyclonal Rabbit anti-Sox17	Millipore (09-038)	1/100
Monoclonal Rabbit S100β Clone EP1576Y	Millipore (04-1054)	1/100

Polyclonal Rabbit Pax 6	Abcam (Ab5790)	1/100
SMA Mouse Monoclonal Clone 1A4	Sigma (A2547)	1/100
Cnn1 1 Mouse Monoclonal Clone hCP	Sigma (C2687)	1/100
Myh11 Mouse Monoclonal Clone 1G12	Abcam (Ab683)	1/100
Alexa Fluor 546 Goat anti-rabbit (H+L)	Life Technologies (A-11035)	1/100
Alexa Fluor 546 Goat anti-mouse (H+L)	Life Technologies (A-11030)	1/100
Alexa Fluor 488 Goat anti-rabbit (H+L)	Life Technologies (A-11008)	1/100
Alexa Fluor 488 Goat anti-mouse (H+L)	Life Technologies (A-11001)	1/100
Alexa Fluor 488 Donkey anti-goat (H+L)	Life Technologies (A-110055)	1/100